IEEE Open Journal of
Vehicular Technology

Received 29 May 2024; accepted 4 July 2024. Date of publication 9 July 2024;
date of current version 24 July 2024. The review of this article was coordinated by Editor Marko Beko.

Digital Object Identifier 10.1109/OJVT.2024.3425061

Large-Scale MIMO Transmitters for CR-NOMA in Fixed Physical Space: The Effect of Realistic System Impairments Using Stochastic Geometry

EMMANUEL AMPOMA AFFUM [1], SAMUEL TWENEBOAH-KODUAH [2], OWUSU AGYEMAN ANTWI [3], BENJAMIN ASUBAM WEYORI [2] (Member, IEEE), AND WILLIE OFOSU [4] (Life Member, IEEE)

[1]Department of Telecommunication Engineering, Kwame Nkrumah University Science and Technology, Kumasi, Ghana
[2]Department of Computer and Electrical Engineering, University of Energy and Natural Resources, Sunyani, Ghana
[3]Department of Telecommunications Engineering, Ghana Communication Technology University, Accra PMB 100, Ghana
[4]Department of Electrical Engineering, Penn State Wilkes-Barre, Pennsylvania, Dallas, PA 18612 USA

CORRESPONDING AUTHOR: SAMUEL TWENEBOAH-KODUAH (e-mail: samuel.tweneboah-koduah@uenr.edu.gh).

ABSTRACT Hardware impairments (HWI) are imperfections in hardware components that diminish wireless communication performance. Unlike Geometric-based Stochastic Models (GBSMs), existing works on the impact of HWI on cooperative-relay (CR) Non-Orthogonal Multiple Access (NOMA) systems employ the Correlated-based Stochastic Model (CBSM), which does not capture realistic propagation mechanisms. Moreover, studies on CR-NOMA with large antenna transmitters (LATs) using CBSM and GBSM have attracted little attention in academia. We consider this as a computational issue. Although considerable work has been done, there is still a significant knowledge gap about how HWI and imperfect successive interference cancellation affect far-users in CR-NOMA with the LAT system. In this study, the LAT is considered a cylindrical array, and parameters such as delay spread, angle of arrival, and departure are incorporated to achieve a CR-NOMA-GBSM system with amplify-and-forward (AF) or decode-and-forward (DF) relaying schemes. To reduce computing demands, we offer a novel concept of using the physical dimensions of the array to derive the location vector of the antenna element. Using Monte Carlo simulation, near and far users' BER performances deteriorate for AF and DF at 15 dB and 5 dB or below, respectively. As far-users can receive comparable performances as near-users for both AF and DF in terms of achievable rates, this demonstrates the potential rewards of CR-NOMA with LAT.

INDEX TERMS Amplify-and-forward (AF), cooperative relay non orthogonal multiple access (CR-NOMA), cylindrical array (CA), decode-and-forward (DF), hardware impairment (HWI), imperfect successive interference cancellation (impSIC), large-antenna transmitters (LATs).

I. INTRODUCTION

Non-Orthogonal Multiple Access (NOMA) is a promising technology for future wireless networks that enables multiple users to share resources simultaneously [1]. NOMA assigns higher power to users with poor channel conditions and exploits successive interference cancellation (SIC) at the receiver to remove multi-user interference [2]. At the transmitter, NOMA utilizes superposition coding by exploiting the power domain to achieve higher spectral efficiency and connectivity [3], [4]. SIC is used to extract the transmitted bit streams from a noisy signal to ensure arbitrary reliability. This is achieved by decoding the signal of a specific user, while treating all other users as noise. The decoded user signal is then re-modulated and subtracted from the received waveform. The process is repeated until all transmitted information streams are demodulated. To address the challenges faced by users with weak signals at the cell edge, cooperative-relay NOMA (CR-NOMA) has attracted significant interest owing to its potential to significantly improve system performance. This innovative technique seamlessly integrates a relay station into the communication process. The transmitter broadcasts a superimposed signal to the relay, which then leverages advanced network coding capabilities, such as amplify-and-forward (AF) and decode-and-forward (DF), to optimize spectral efficiency, reliability, and fairness for all users. The relay then re-transmits the enhanced signal to cell-edge users with improved quality [5], [6]. In AF relaying, the relay amplifies the signal received from the source and transmits it to the destination(s), thereby improving both signal strength and security without the need to obtain precise channel state information (CSI) [7], [8]. In contrast, for DF relaying, the relay decodes the received signal and re-encodes it before forwarding it to the destination(s). It also performs error correction and interference mitigation [9] and exploits spatial diversity when utilized in a multi-relay system [10].

The information-theoretic capacity, which is influenced by factors such as signal-to-noise ratio (SNR), spatial correlation in the propagation environment, precise channel estimation, quality of transceiver hardware, and availability of signal processing resources, limits the spectral efficiency of wireless links [11], [12]. To overcome these limitations and achieve the necessary performance for fifth-generation (5G) networks, the large antenna transmitters (LATs) or massive multiple-input multiple-output (MIMO) systems, have been developed. When combined with CR-NOMA [13], these approaches have the potential to increase the spectral efficiency and enhance diversity gain [14]. LATs are key technologies in 5G networks that use a large number of antennas at as a base station (BS) to simultaneously serve multiple users. LATs unlock several key benefits, such as 1) mitigation of propagation losses, 2) decreasing interference leakage, 3) optimal low-complexity algorithms, 4) inter-user interference mitigation, 5) high beamforming resolution, and 6) asymptotic upper capacity for enhanced spectral efficiency in 5G networks. [15], [16] [17], [18].

In practice, hardware impairments (HWI) are predominantly caused by low cost hardware components that are inherently susceptible to various impairments. These include: 1) amplifier non-linearities, which can lead to signal clipping and spectral regrowth, resulting in increased inter-modulation distortion and interference [19]; 2) in-phase/quadrature (I/Q) imbalance: this imbalance between the in-phase and quadrature components of the signal can induce phase errors and diminish signal power [19], [20]; 3) phase noise: random fluctuations in the carrier signal's phase can cause jitter and symbol timing errors [20], [21]; and 4) quantization errors, which can introduce noise and distortion, especially for low-resolution converters [19], [21]. Transmitter/receiver systems consist of distinct hardware components including amplifiers, converters, mixers, filters, and oscillators. Each of these components introduces unique imperfections and signal distortions, which are inevitable [22]. These distortions impair signal quality, resulting in reduced data rates and increased probability of errors [19]. Hence, in system design, cost or power reduction often allows some level of impairment, which results in a trade-off between cost and performance, power consumption, and complexity. This trade-off necessitates a careful system design that considers application requirements, cost constraints, and desired performance levels. During the design stage, the non-ideal behavior of each component can be meticulously modeled to create and implement compensation algorithms. By accurately capturing the behavior of non-ideal components, such as the frequency response, noise characteristics, and non-linearity, designers can develop compensation algorithms that effectively counteract their detrimental impacts. Although compensation algorithms can generally reduce impairments through analog and digital signal processing, residual impairments persist [23], [24], [25], [26]. These impairments have been found to limit the full performance and reliability of wireless communication systems, particularly in high-speed and high-capacity network applications, where high signal quality is required [24]. Therefore, further research and development in this area is essential.

A three-dimensional (3D) Geometric-based Stochastic Model (GBSM) is a channel model that leverages the 3D characteristics of the propagation environment [27], [28]. This model incorporates the stochastic nature of wireless channels by employing realistic spatial distributions, well defined geometric parameters, and random variables [28]. This approach enables the GBSM to accurately model various channel properties, including the path loss, shadowing, fading, direction of arrival, and delay spread of multipath components [27]. By incorporating these factors, 3D GBSM surpasses theoretical Correlated-based Stochastic Mode (CBSM) models in its ability to provide a more accurate and realistic representation of real-world wireless channels [29], [30]. This is important for designing and evaluating the performance of communication systems in diverse scenarios encompassing vehicle-to-vehicle communication, drone-based networks, CR-NOMA, and massive MIMO systems [29]. Although there has been much research on LATs, little is known about how transceiver hardware problems or HWI affect LATs CR-NOMA systems with 3D GBSM channel models. This is a major knowledge gap because these problems can significantly affect the performance and usability of practical GBSM-based CR-NOMA systems. Moreover, there is a paucity of studies on analyzing system impairment factors in CR-NOMA networks using LATs and 3D GBSM channel models. Existing literature only considers ideal transceiver hardware and perfect SIC, whereas practical systems are affected by HWI. These impairments, which increase the system error rate, and complexity, and decrease signal quality, and spectral efficiency have not been fully addressed.

In [31], the effect of antenna element spacing of a uniform rectangular array (URA) on an ideal LAT CR-NOMA network was compared with a similar system using a theoretical CBSM. It was found that increasing the element spacing improves the CR-NOMA system in terms of the bit-error rate (BER), outage probability, and achievable rate. However, practical CR-NOMA implementations face HWI and imperfect SIC (impSIC) challenges that must be addressed. In realistic scenarios, HWI and impSIC can degrade system performance [21], [32], [33], [34]. An impSIC is caused by channel estimation errors, feedback delays, and computational constraints, which can significantly degrade the performance of CR-NOMA systems [35]. During SIC decoding, the distortion is successively amplified, causing failed decoding and error propagation [36]. The near user (NU) signal interferes with the far user (FU) in NOMA and must be canceled by SIC before decoding [36], [37], [38]. The relay also forwards its distortion, further polluting the signals that users receive [39], [40]. These issues exacerbate CR-NOMA performance as the relay amplifies the interference of the NU. In this case, the FU is most affected since it experiences interference from the decoding errors of the NU [38]. Han W. et al. [41] demonstrated that HWI and impSIC could cause a reduction of over 20% in the sum rate and error performance of CR-NOMA networks. The authors in [42] showed that cell-edge users can experience a reduction in the data rate of up to 35–40% owing to certain effects. Analytical studies have found that outage probability increases exponentially with increasing HWI and SIC error levels [43]. Moreover, user fairness is affected, with the rate of FUs being more severely degraded [38].

In [32], the authors found that these impairments can lead to an error floor in the outage probability. However, a media-based modulation (MBM)-aided scheme that is robust to such impairments was proposed in [33]. Arzykulov et al. [21] extended this study, highlighting the need for an optimal power allocation scheme to ensure fairness in the presence of HWI. In the context of the Internet of Things (IoT), the effect of HWI on NOMA users and the proposal of an adaptive transmission strategy at the relay node were investigated in [39]. The authors of [44], [45], and [39] in their work have found that these impairments could significantly affect system performance, particularly user fairness.

A comprehensive analysis of the effects of HWI on NOMA dual-hop relaying networks focusing on the limitations imposed by distortion noise was conducted in [36] and [46]. The authors in [36] found that residual HWI and impSIC have a negative impact on system performance, with impSIC having a more pronounced effect than residual HWI. The authors in [20] demonstrated that the outage performance of the cooperative NOMA scenario exceeds that of non-cooperative NOMA in the high-SNR regime when investigating the impact of residual transceiver HWI. In a secure cooperative NOMA system, Li Meiling et al. [47] found that residual HWI affects both legitimate users and eavesdroppers by increasing the outage probability and decreasing the intercept probability over multipath fading channels. In [48], the authors found that systems with power-splitting relaying (PSR) demonstrate better performance than those using time-sharing relaying (TSR) methods.

The authors of [49], [50], [51] highlighted the significance of HWI in practical cooperative NOMA systems, emphasizing their effects on transceivers at BS, relay nodes, and user nodes. Table 1 summarizes recent related studies on system impairment factors and performance of CR-NOMA systems using the theoretical CBSM channel model.

A. MOTIVATION

Although previous studies have emphasized the significance of HWI and impSIC in CR-NOMA systems using theoretical CBSM and single antennas systems, the limitations of this approach are evident in [62] and [63]. The CBSM does not consider critical propagation parameters, such as path loss, delay spread (DS), delay profile, and angle of arrival (AoA), which accurately reflect real-world conditions. In contrast, GBSM includes these factors and accurately models and evaluates the realistic behavior of LAT systems in practical scenarios [64], [65], [66]. However, there is a noticeable gap in the literature regarding the examination of the impact of system impairments in the context of LATs CR-NOMA systems using 3D GBSM. Therefore, it is crucial to investigate and understand the practical implications of these systems under real-world conditions. Our initial research in [67] and [68] investigated CR-NOMA with LATs, using the GBSM channel model. Specifically, we explored the impact of the proposed 3D channel model on system performance, offering a realistic and practical representation of the propagation characteristics of LAT systems within the considered propagation environment. Subsequently, in [31], we examined the influence of the LAT antenna element spatial correlation or inter-element spacing on a CR-NOMA system under AF and DF network coding schemes. As per the authors, this research is incomplete if the impact of LAT hardware impairment and imperfect SIC on the CR-NOMA using GBSM system is not examined.

B. CONTRIBUTIONS

The effect of HWI on a two-stage CR-NOMA with LAT using GBSM is examined in this work. The LAT in this analysis is modeled as CA because the radiated signals can be accurately regulated in three dimensions, enhancing system capacity. Again, scanning acceleration and space-time signals can be employed by the CA to decrease clutter. and additionally, in the horizontal plane, the CA enables the creation of directed beams in any direction or an omni-directional pattern. The 3D GBSM model under discussion adds the elevation angle of the antenna boresight θ_{tilt} in the channel equation, in contrast to the 2D channel models where the antenna boresight is fixed and the channel's degree of freedom in the elevation is not being exploited. As a result, the downtilt angle's dynamic fluctuation can reveal various 3D beamforming opportunities that could result in notable performance gains. To facilitate efficient channel estimation for a potentially large number of antennas in the cylindrical array (CA), we employed a time-duplex division (TDD) protocol [69], [70] for

TABLE 1. Summary of Related Work on CR-NOMA With HWI

Ref.	Coding Scheme	Antenna Type	Channel Model	Performance Metrics	Contributions
[19]	DF	Single antenna	Nakagami-m (CBSM)	BER & outage probability	Provided an analytical framework for BER and outage probability performance analysis under system impairment factors that impact performance.
[21]	DF	Single antenna	Rayleigh (CBSM)	Outage probability, throughput & spectral efficiency	Derived end-to-end outage probability and investigated the performance of a cooperative NOMA network in the presence of system impairments and interference.
[52]	AF	Single antenna	Nakagami-m (CBSM)	Outage probability & throughput	Showed that error floor of the outage probability is caused by RHIs and imperfect CSI, and optimal power allocation could improve performance.
[53]	DF	Single antenna	Rayleigh (CBSM)	outage probability, ergodic rate, spectral efficiency & energy efficiency	Derived a closed-form expressions for the outage probability, spectral efficiency and energy efficiency of reflective intelligent surface (RIS)-aided NOMA under impairment with full-duplex relay.
[54]	DF	Single antenna	Rayleigh (CBSM)	Outage probability	Investigated the performance improvement of cognitive radio-inspired NOMA system with relay selection strategies under HWI. Examine closed-form outage probability analysis of the selection strategy.
[55]	DF & AF	Single antenna	Rayleigh (CBSM)	Outage probability & throughput	Provided analytical framework to examine impact of hardware noise and imperfect SIC operation on AF NOMA networks.
[56]	AF	Single antenna	Rayleigh (CBSM)	outage probability & ergodic capacity	Analyzed outage and throughput performance of a NOMA system using AF relaying under HWI and imperfect SIC.
[57]	DF	Single antenna	Rayleigh (CBSM)	Outage probability, BER & minimum throughput	Proposed a new resource management framework for backscatter-aided cooperative NOMA under imperfect SIC where a combination of the bisection method and dual theory was used to achieve performance equivalent to brute-forcing search technique.
[33]	DF with MBM	Uniform linear antenna array (ULA) at the BS, single antenna relay & user devices	Rayleigh (CBSM)	BER	Proposed a media-based modulation (MBM)-aided uplink cooperative NOMA under HWI and imperfect CSI
[58]	AF	Single antenna	Nakagami-m (CBSM)	Outage probability	Analyzed the performance of cooperative SWIPT NOMA for massive IoT systems under residual HWI and channel estimation errors with optimal relay selection protocol
[59]	AF	ULA at the BS, single antenna relay and user devices	Rayleigh (CBSM)	Capacity, sum rate & SINR	Derived exact closed-form SINR expressions of the capacity and sum rate. Noted that increasing number of antennas improves performance.
[60]	DF	Single antenna BS & user devices, multi-ULA antennas at the relay	Rayleigh (CBSM)	Energy efficiency & spectral efficiency	Investigated the impact of HWI on the MIMO full-duplex relaying and end-to-end achievable rate.
[61]	DF	Single antenna	Rayleigh (CBSM)	EC, outage probability & bit-error probability (BEP)	Introduced reversed DF relaying NOMA and provided upper bound for EC, asymptotic and lower bound expressions for outage probability, exact closed-form BEP expression with imperfect CSI.
Our work	AF & DF	Cylindrical antenna array at the BS, single antenna relay & user devices	3D GBSM	Bit-error rate, outage probability, & acheivable rate	This study introduces a 3D 3D GBSM channel and LATs into a CR-NOMA system with HWI and impSIC. The performance of the proposed system is evaluated under practical impairments, considering the proposed realistic channel model.

downlink (DL) transmission, leveraging channel reciprocity for instantaneous CSI. The accuracy of the acquired CSI depends on factors such as the channel dynamics and antenna configuration [71].

Our idea is illustrated by deriving the array response of the CA and integrating it into the 3D GBSM model to provide the channel coefficients between the LAT and the Relay. Our approach is new in that, to reduce computing complexity, we estimate the antenna placement vector in the array response using the physical dimensions of the CA. At this early level of the investigation, we restricted our analysis to AF and DF coding schemes to relay the transmitted signal to the user. The main idea of CR-NOMA is to improve the far-user's performance, hence, channel quality was emphasized to distinguish users, giving priority to users with stronger links to the fixed relay. Given this, we investigate the impact of HWI and impSIC on the bit error (BER), outage probability, and achievable rate of the FU to NU. The main contributions are summarized as follows:

- We proposed a two-stage CR-NOMA using GBSM at both the transmitter and the relay to examine the impact of HWI and impSIC on users, with the transmitter modeled as a CA.
- We derive a new channel realization for the proposed model between the transmitter and relay by estimating the array response of the CA and incorporating it in the 3D GBSM model under consideration. To lessen computational challenges, we present a new idea of estimating the antenna element location vectors of the transmitter using the physical dimension of the antenna array.
- To improve the performance regarding BER, OP, and achievable rates of far-users the AF or DF coding schemes are used at the relay.
- Our findings show that near and far-users can attain similar BER concerning AF by maintaining SNR at 15 dB or less, On the other hand, with DF, far-user performance improvements start at 5 dB. Furthermore, in terms of outage probability, the performances remain consistent for both DF and AF across all scenarios of impairment. The smallest performance difference was observed for DF after 20 dB. Nonetheless, both individuals' performance was very stable when using AF. Last but not least, the results of the achievable rate analysis for AF and DF show the possible benefits of LAT CR-NOMA systems employing GBSM as far-users can obtain similar rates for both AF and DF at different SNRs as near-users.

C. PAPER ORGANIZATION

The remainder of this paper is organized as follows. Section II presents the signal and system modeling. Section III analyze the impact of HWI and impSIC on the performance of CR-NOMA systems. Section IV presents numerical results and discussion. Finally, Section V concludes the paper.

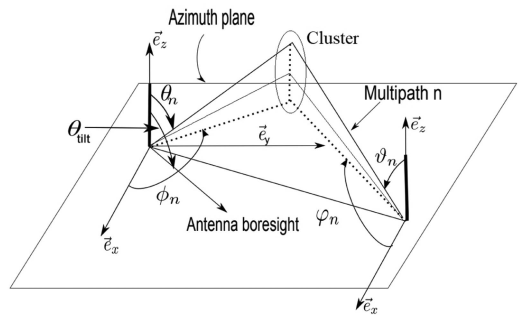

θ_{tilt} = Elevation angle of the boresight
θ_n, ϑ_n = Elevation AoD & AoA of the n^{th} path respectively
ϕ_n, φ_n = Azimuth AoD & AoA of the n^{th} path respectively

FIGURE 1. 3D channel model for large-scale MIMO system with a single cluster. Angles of arrival (AoA) and departure (AoD) are depicted for the *n*th path.

The symbols and notations used throughout this paper are summarized in Table 2.

II. SIGNAL AND SYSTEM MODELING

A. 3D GBSM CHANNEL MODELING

A 3D channel model is proposed here based on the 3GPP standard [72], [73], [74]. A key advantage of the 3D GBSM is that it can provide a detailed characterization of the wireless channel, including spatial correlations and interference patterns. This model can be used to simulate the propagation of radio waves in a wireless environment and to predict the performance of wireless systems under different conditions. Additionally, the model considers the effects of large antenna arrays, which can result in complex spatial correlations and interference patterns.

In this study, a LAT antenna was modeled as a CA that captures the main characteristics of the 3D channel, such as the DS, AoA, angle of departure (AoD), elevation angle of arrival (EoA), and elevation angle of departure (EoD) [63], [75], [76]. Moreover, the model incorporates the elevation angle of the antenna boresight into the channel and to enable dynamic adjustment of the antenna's downtilt angle θ_{tilt}. This enhances the 3D beamforming performance and improves system efficiency [77]. Fig. 1 shows a schematic of the 3D channel model, indicating the various parameters required for the GBSM modeling. For this model, the path loss and large-scale characteristics, such as DS, elevation spread at departure (ESD), elevation spectrum at arrival (ESA), azimuth spectrum at departure (ASD), azimuth spectrum at arrival (ASA), shadow fading (SF), and Rician factor, are created for each user based on the statistical distributions specified according to the 3GPP standard. In the 3D channel model, small-scale parameters, such as power levels, delays, AoDs, AoAs, and cross-polarization ratios (XPRs), were generated for each propagation path. These parameters are influenced by the large-scale parameters of the model.

TABLE 2. List of Symbols and Notations

Notation	Meaning or Description
U1, U2	User 1 (Near user, NU), User 2 (Far user, FU)
P_i	Transmit power at node $i = s, r$
α_i	Power allocation at the source for user i
$s_i(t)$	Modulated baseband signal of user i
$\mathbf{H}^{3D}_{s,u}$, $\mathbf{H}^{CA}_{s,u}$	3GPP's generic and proposed 3D GBSM channel matrix. h_j is 3D GBSM channel coefficient, $j = t, i$
(ϕ^{AoD}_n), (θ^{AoD}_n)	Azimuth and elevation AoD of the n^{th} path
(φ^{AoA}_n), (ϑ^{AoA}_n)	azimuth and elevation AoA of the n^{th} path
θ_{tilt}	Downtilt angle of the transmitting antenna
G^{3D}_i	Antenna array gain, $i =$ TX, RS
G^j_H	Antenna radiation pattern, $j =$ H, V
ϕ_{3dB}, θ_{3dB}	Horizontal, and vertical HPBW
κ_n	Complex random amplitude of the n^{th} path
P_n	Power of the n^{th} path
σ_{SF}	Lognornal shadow fading
h_i	3D GBSM channel coefficient, $i = t, 1, 2$
a_{TX}, a_{RX}	Transmitter and receiver antenna response
$\mathbf{k}_i = k\hat{\mathbf{v}}$	Wave vector, $i = t, r$. $\hat{\mathbf{v}}$ is Wave propagation direction. λ is wavelength
$\varkappa_i$	Path loss from the source to the relay and from the relay to user $i = t, 2, 3$
κ_i	Level of impairment at $i = t, r$
η_j	Distortion noise, $j = t, r, i$
η	Aggregate level of impairment
n_j	Additive white Gaussian noise (AWGN), $j = r, i$
ϱ	Propagation distance dependent non-fading gain
ℓ	Channel estimation error
ζ	Effect of impSIC
$\mathbb{CN}(\cdot)$	Complex normal distribution operator
$\lvert . \rvert$	Absolute value
d_1, d_2	Aggregate distortion for first and second hops of CR-NOMA
$\mathbb{E}(\cdot)$	Expectation operation
$Q(\cdot)$	Q-function operator
G	AF amplification gain
σ_R	Complex noise power
$\eth^k_i$, ς^k_i	SDNR, SINR for user i, $k =$ AF, DF
y^k_i	Received signal at user i, $k =$ AF, DF
P^k_i	Outage probability of the i^{th} user, $k =$ AF, DF
$P^{impSIC}_{1,k}$	Outage probability with impSIC, $k =$ AF, DF
ρ	Average SNR
R^k_i	Achievable rate of user i, $k =$ AF, DF. $R^{impSIC}_{1,k}$ is rate for user 1 with impSIC
$\hat{R}_i$	Target rate of user i (QoS requirement)

According to the 3GPP model, the effective channel between the sth transmitter (TX) antenna port with M subpaths and the uth receiver antenna port [78], [79] is given in (1), shown at the bottom of the next page, where κ_n is the complex random amplitude of the nth path and $s = 1, \ldots, N_{TX}$, $u = 1, \ldots, N_{RX}$ are the numbers of transmit and receiver antenna elements, respectively. $(\phi^{AoD}_n, \theta^{AoD}_n)$ are the azimuth and elevation AoDs, respectively. Here, $(\varphi^{AoA}_n, \vartheta^{AoA}_n)$ are the azimuth and elevation AoA of the nth path, respectively. The TX antenna gain is given by

$$G^{3D}_{TX}\left(\phi^{AoD}_n, \theta^{AoD}_n, \theta_{tilt}\right) \approx G^{TX}_H\left(\phi^{AoD}_n G^{TX}_V(\theta^{AoD}_n, \theta_{tilt})\right) \quad (2)$$

From (1), the responses of the antenna array are $a_{TX}(\phi^{AoD}_n, \theta^{AoD}_n)$ and $a_{RX}(\varphi^{AoA}_n, \vartheta^{AoD}_n)$. Following the approach in [72], the precise 3D antenna radiation patterns in both the horizontal (G^{TX}_H) and vertical (G^{TX}_V) planes are expressed as [78]

$$G^{TX}_H(\phi^{AoD}) = -12\left(\frac{\phi^{AoD}}{\phi_{3\,dB}}\right)^2 \quad (3)$$

and

$$G^{TX}_V(\theta^{AoD}, \theta_{tilt}) = -12\left(\frac{\theta^{AoD} - \theta_{tilt}}{\theta_{3\,dB}}\right)^2 \quad (4)$$

where ϕ^{AoD} is the horizontal azimuth angle between the user and array boresight; θ^{AoD} is the vertical elevation angle between the user and array boresight; and $\phi_{3\,dB}$ and $\theta_{3\,dB}$ are the horizontal and vertical half-power beamwidths (HPBWs), respectively. The 3D channel model includes the elevation dimension and considers the directional radiation patterns of active antenna elements. This model expresses the channel between the BS and each user as a function of propagation paths and associated physical parameters. In this study, a new 3D GBSM channel was generated by using a generic 3GPP model. The array response of the model was modified by incorporating antenna element location vectors that were defined based on the physical dimensions of the array. Algorithm 1 outlines the procedure for estimating the location vectors of the CA elements for the array responses in (1). Considering the CA in Fig. 2, the adjacent elements are separated by a d_z wavelength on the z-axis and located at a radius of the ρ_r wavelength from the center (z-axis) with respect to the xy plane. From the center axis, the antenna elements were separated by $\rho_r d\phi$ on the circumference forming a ring in cylindrical coordinates. A CA can be modeled by wrapping a URA around a virtual cylinder, as shown in Fig. 2. The URA is composed of A-elemental uniform linear array (ULA) in the z direction and B-element on the xy plane [80]. In this case, the position vector of the sth transmitting antenna element can be calculated by identifying the location of the mth uniform circular array (UCA) along the z-axis and the angular location of the nth element on the mth UCA in the xy plane. Here, $m = 1, \ldots, M$ represents the total

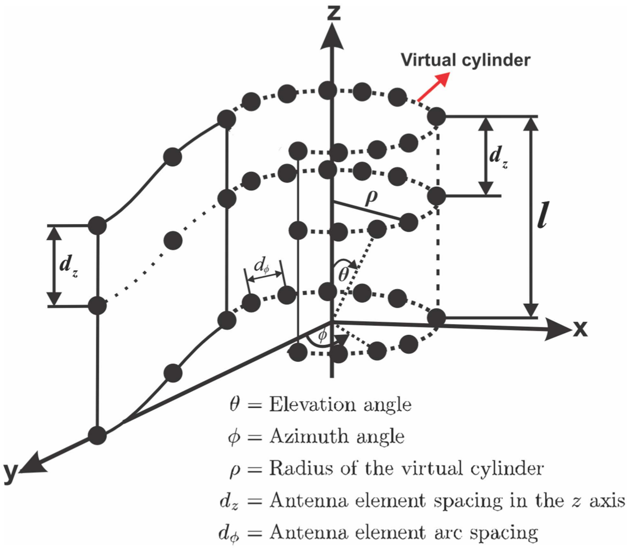

FIGURE 2. Structure of cylindrical array with elements distributed in the *xy*-plane with *z*-axis as the origin, modeled as wrapping a URA about the axis.

number of UCA elements along the z-axis, and $n = 1, \ldots, N$ represents the total number of antenna elements in each UCA. Thus, the array dimension of the CA is specified as $l = 4\lambda$, from which the radii of both the virtual cylinder and the UCA are computed as $\rho_r = 4\lambda/l$. Moreover, by defining $d_z = 4\lambda/M$ wavelength as the distance between the initial and secondary UCA along the z-axis, the position of the remaining UCAs on the z axis can be determined as $4\lambda(m-1)/M$ wavelengths, as shown in Fig. 2. From the figure, the scalar product of each antenna element is given by:

$$\mathbf{v}_t \cdot \mathbf{x}_s = \cos(\phi - \varphi_s)\sin(\theta) \quad \text{and}$$
$$\mathbf{v}_r \cdot \mathbf{x}_u = \cos(\varphi - \upsilon_u)\sin(\vartheta) \tag{5}$$

where the angular position of the nth element of the mth UCA with N_{TX} number of transmit ports on the xy plane is given by $\varphi_s = \frac{2\pi(s-1)}{N_{TX}}$, $s = 1, .., N_{TX}$, whereas that of the receiver port with N_{RX} is $\upsilon_u = \frac{2\pi(u-1)}{N_{RX}}$, $u = 1, \ldots, N_{RX}$. $\mathbf{x}_s$ is the location vector of the sth transmit antenna, $\mathbf{x}_u$ is the location vector of the uth receive antenna, and $\mathbf{k}_t$ and $\mathbf{k}_r$ are the transmitter and receiver wave vectors, respectively.

Given that, $\mathbf{k} = k\hat{\mathbf{v}}$, where $k = 2\pi/\lambda$ is the carrier wavelength and $\hat{\mathbf{v}}$ is the direction of wave propagation, the CA antenna array response of the sth transmit port is given by:

$$a_t(\varphi_n, \theta_n) = \exp(i\mathbf{k_t} \cdot \mathbf{x_n})$$
$$= \exp\left(ik\rho\frac{4\lambda(m-1)}{M}\cos(\phi_n - \varphi_s)\sin(\theta_n)\right) \tag{6}$$

Algorithm 1: Estimating Location Vector of Cylindrical Antenna Array (CA).

Start
Read CA input parameters
Set antenna spacing by d_z wavelength on the z-axis
Locate elements at a radius ρ_r wavelength from the center
Model CA as a URA wrapped around a virtual cylinder
for all transmitting antenna elements **do**
  Identify the location of the UCA along the z-axis
  Identify the angular location on the xy plane
  Calculate the array dimension $l = 4\lambda$
  Compute the radius as $\rho_r = \frac{4\lambda}{l}$
  Define the distance between UCA groups as $d_z = \frac{4\lambda}{M}$
  Determine the position of remaining UCAs on the z-axis
  for all antenna elements in the UCA **do**
    Calculate the location vector
    for all transmit port on the xy plane **do**
      Calculate the array response
    end for
  end for
  for all receive port **do**
    Calculate the array response
  end for
end for
End

where $m = 1, \ldots, M$ is the number of array rings in the z direction, and the response at the receiving antenna uth is given by

$$a_u(\varphi_n, \vartheta_n) = \exp(ik(u-1)d_r\sin(\varphi_n)\sin(\vartheta_n)) \tag{7}$$

where $u = 1, \ldots, N_R$ represents the number of antennas at the receiver.

In this study, the transmitter antenna is modeled as a CA that serves as a single-antenna relay with a half-duplex connection. The path between TX and relay-station (RS) has a single bounce cluster, resulting in N paths. From the analysis in (6) and (7), the final 3D GBSM channel model of the proposed model in Fig. 3 between a single antenna receiving port uth and a CA transmitter's transmit antenna port sth [78] is given in (8), shown at the bottom of the next page, where P_n denotes the power of the nth path and σ_{SF} is the lognormal shadow fading of the nth path. N is the number of propagation paths, M is the number of subpaths per path, d_r is the separation between the receiving antenna

$$\mathbf{H}_{s,u}^{3\text{D}} = \sqrt{\frac{P_n\sigma_{SF}}{M}}\sum_{n=1}^{N}\kappa_n\left[\begin{array}{l}\sqrt{G_{TX}^{3\text{D}}\left(\phi_n^{AoD}, \theta_n^{AoD}, \theta_{tilt}\right)}\sqrt{G_{RS}^{3D}\left(\varphi_n^{AoA}, \vartheta_n^{AoA}\right)} \\ \times\left[a_{RX}\left(\varphi_n^{AoA}, \vartheta_n^{AoA}\right)\right]_u\left[a_{TX}\left(\phi_n^{AoD}, \theta_n^{AoD}\right)\right]_s\end{array}\right] \tag{1}$$

ports, k is the wave number, and G_{RS}^{3D} is the gain of the relay antenna. Moreover, the model incorporates the elevation angle of the boresight of the antenna into the channel and enables dynamic adjustment of the antenna's downtilt angle θ_{tilt} to enhance the 3D beamforming performance and improve system efficiency [77].

B. SYSTEM MODEL

In this section, **we** analyze a GBSM-based CR-NOMA system with HWI and impSIC in which the transmitter is modeled as a CA. To ensure the reliability of edge users, networking schemes such as AF and DF were employed at the relay node as indicated in Fig. 3. The figure illustrates a wireless communication system in which a BS transmits to two users, the NU as *U1* and the FU as *U2*, via an AF or DF relay. This demonstrates the concept of CR-NOMA with impSIC and HWI, where there is no direct link between the BS and the users. The operation of the system is based on NOMA concepts, which employ superposition coding to combine *U1* signal $s_1(t)$ and *U2* signal $s_2(t)$ at the BS. These signals have varying power allocations based on the channel gain, ensuring that $\mathbb{E}[|h_2|^2] < \mathbb{E}[|h_1|^2]$, without loss of generality. Accordingly, the power coefficients of *U1* and *U2* were α_1 and α_2, respectively. Thus, the transmitted superimposed signal is thus $s(t) = \alpha_1 s_1(t) + \alpha_2 s_2(t)$, with $\alpha_1 < \alpha_2$ and $\alpha_1 + \alpha_2 = 1$. The received signal at the relay under ideal conditions is given by

$$y_r = h_t \sqrt{\varkappa_t P_s} s(t) + n_r \tag{9}$$

where h_t is the channel coefficient described in (8) and $\varkappa_t$ is a distance dependent path loss between the BS and the relay [81], n_r is the additive white Gaussian noise (AWGN) with a zero mean.

However, in the presence of system impairments, the relay node receives a noisy version of $s(t)$ given by

$$y_r = h_t(\sqrt{\varkappa_t P_s} s(t) + \eta_t) + \eta_r + n_r \tag{10}$$

where η_t, η_r are the additive distortion noises. These noises are ergodic stochastic processes generated by the HWI at the BS and relay. Distortion noise refers to the modification of the desired signal, whereas traditional receiver noise represents random variations in the electronic circuit of the receiver. A key distinction is that the power of the distortion noise is non-stationary because it is directly proportional to both the signal power and the channel gain. The proportionality coefficients κ_t and κ_r, outline the degree of impairment and are associated with the Error Vector Magnitude (EVM) requirement specified in the 3GPP standard. The correlation emphasizes the critical role that these coefficients play in the overall system performance. The distortion noise can be modeled as follows:

$$\eta_t \sim \mathbb{CN}(0, \kappa_t^2 P_s), \quad \eta_r \sim \mathbb{CN}\left(0, \kappa_r^2 P_s |h_t|^2\right), \tag{11}$$

where κ_t^2, $\kappa_r^2 \geq 0$ represent the design parameters that characterize the HWI levels at the transmitter and receiver, respectively. The Gaussianity of distortion noise is motivated by the central limit theorem, which describes the aggregate effect of several HWI. From this, (10) can be expressed as

$$y_r = h_t \left(\sqrt{\varkappa_t P_s} s(t) + \eta\right) + n_r, \tag{12}$$

where $\eta \sim \mathbb{CN}(0, \kappa^2 P_s)$ is the aggregate effect of the impairment in the system, and $\varkappa_t$ is the path loss exponent between the source and relay. The overall impairment level is $\kappa = \sqrt{\kappa_t^2 + \kappa_r^2}$. According to [82], for a given channel realization, the power of the aggregate distortion at the receiver is given by

$$\mathbb{E}_{\eta_t,\eta_r}\{|h_t \eta_t + \eta_r|^2\} = P_s |h_t|^2 (\kappa_t^2 + \kappa_r^2). \tag{13}$$

κ_t and κ_r parameters are EVM, which is the ratio of the average distortion magnitude to the signal magnitude used to evaluate the radio-frequency transceivers. It measures the overall effects of HWI and the compensation algorithms. Upon receiving the transmitted signal from the source, the relay has two options, as shown in Fig. 3, for forwarding the signal to all users:

1) *AF:* The relay amplifies the noisy signal using a gain factor and transmits it. Here, the relay applies an amplification gain factor of G to y_R. This gain is given by

$$G = \sqrt{\frac{P_r \varrho^2}{P_s |h_t|^2 \left(1 + \kappa_t^2\right) + P_s \left(1 + \kappa_t^2\right) \ell^2 + \sigma_R^2}} \tag{14}$$

where P_r is the relay's transmit power, ϱ is non-fading variable gain that depends on propagation distance, and ℓ is the channel estimation error model as additive Gaussian noise.

The received signal at user i, either *U1* or *U2*, from the relay is expressed as,

$$\begin{aligned} y_i^{AF} &= h_i \left(G\sqrt{\varkappa_i P_r} y_r + \eta_i\right) + n_i \\ &= h_{r,i}\left[G\sqrt{\varkappa_i P_r} h_t \left(\sqrt{\alpha_t P_s} s(t) + \eta\right) + \eta_i + n_r\right] \\ &\quad + n_i. \end{aligned} \tag{15}$$

$$\mathbf{H}_{s,u}^{\mathrm{CA}} = \sqrt{\frac{P_n \sigma_{SF}}{M}} \sum_{n=1}^{N} \kappa_n \begin{bmatrix} \sqrt{G_{TX}^{\mathrm{3D}}\left(\phi_n^{AoD}, \theta_n^{AoD}, \theta_{tilt}\right)} \\ \times \exp\left(ik\rho(4\lambda(m-1)/M)\cos(\phi_n^{AoD} - \varphi_s)\sin\theta_n^{AoD}\right) \\ \times \sqrt{G_{RS}^{3D}\left(\varphi_n^{AoA}, \vartheta_n^{AoA}\right)} \exp\left(ik(u-1)d_r \sin\varphi_n^{AoA} \sin\vartheta_n^{AoA}\right) \end{bmatrix} \tag{8}$$

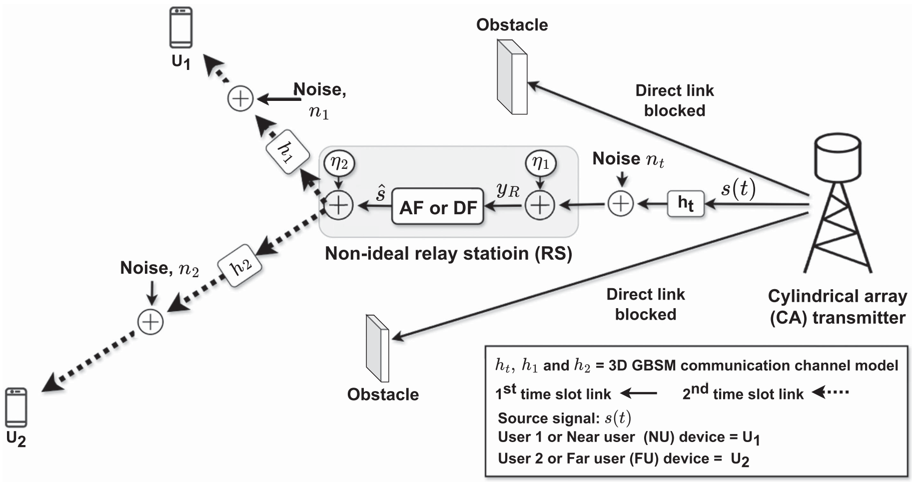

FIGURE 3. Proposed system subject to under hardware impairment and imperfect SIC

2) *DF:* The relay first decodes the constituent signals $s_1(t)$ and $s_2(t)$ from the noisy version of $s(t)$. It then regenerates and re-encodes these signals separately, before combining and forwarding them. The received signal at the user device after the DF coding scheme is given by,

$$y_i^{DF} = h_i\sqrt{\varkappa_i P_r}\,(s_1(t) + s_2(t) + \eta_i) + n_i. \tag{16}$$

where $\varkappa_i$ is the relay to the ith user path loss.

III. PERFORMANCE ANALYSIS

For user *U1*, signal detection is performed by treating $s_2(t)$ as noise. *U1* experienced better channel conditions than *U2*. Thus, $s_1(t)$ can be reliably detected by leveraging the power disparity between $s_1(t)$ and $s_2(t)$.

User *U2*, on the other hand, sees high interference from $s_1(t)$ because of its poor channel. To mitigate this, SIC is first performed to remove $s_1(t)$ from the received signal. This process involves detecting and subtracting an estimate of $\alpha_1 s_1(t)$ from the received signal. However, because of channel uncertainties and noise, the SIC process is imperfect, and residual interference remains. After SIC, *U2* detects its signal $s_2(t)$ by treating the remaining distortion as additional noise. In the proposed systems, imperfect cancellation degrades *U2*'s signal detection compared to an ideal NOMA system. The performance analyses of the system under AF and DF coding schemes are as follows.

A. APPLICATION OF AF CODING SCHEME

Under perfect system conditions, at the receiving end, an SIC is used to reduce the interference between users. Without loss of generality, the SIC decoding order is determined by the effective channel gains, which are generally in ascending order, that is, $|h_1|^2 \geq |h_2|^2$. According to [55] and [83], the signal-to-interference plus noise ratio (SINR) for *U1* to decode $s_2(t)$ through perfect SIC processing can be expressed as:

$$\varsigma_{2\to 1}^{AF} = \frac{\alpha_2\rho|h_t|^2|h_1|^2}{\alpha_1\rho|h_t|^2|h_1|^2 + |h_t|^2 + |h_1|^2 + \frac{1}{\rho}}. \tag{17}$$

After *U2*'s message has been decoded and removed, *U1* decodes its own signal by matching the SINR (ς_1^{AF}) between the relay and *U1*. The SINR is given by,

$$\varsigma_1^{AF} = \frac{\alpha_1\rho|h_t|^2|h_1|^2}{|h_t|^2 + |h_1|^2 + \frac{1}{\rho}}. \tag{18}$$

The SINR (ς_2^{AF}) between the relay and the *U2*, to detect its own message, is given by

$$\varsigma_2^{AF} = \frac{\alpha_2\rho|h_t|^2|h_2|^2}{\alpha_1\rho|h_t|^2|h_2|^2 + |h_t|^2 + |h_2|^2 + \frac{1}{\rho}} \tag{19}$$

The SINR of the effect of impSIC on the proposed system with a perfect transceiver can be expressed as:

$$\varsigma_{2,AF}^{impSIC} = \frac{\alpha_1\rho|h_t|^2|h_1|^2}{\rho\zeta^2 + |h_t|^2 + |h_1|^2 + \frac{1}{\rho}} \tag{20}$$

where $\rho = P_r/\sigma^2$ gives the average SNR, and ζ is the effect of impSIC.

The effect of HWI on the system performance using the AF coding scheme is analyzed by considering the signal-to-noise plus distortion ratio (SNDR). When dealing with imperfect hardware, it is critical to analyze the system while also considering the residual HWI. Although the focus is on how these impairments can negatively impact performance, it is equally important to analyze how imperfections affect the system performance when users communicate through an AF relay in a NOMA relaying network. The SNDR, $\eth_2^{AF}$ at *U2* to detect its own signal, is expressed in [55] as

$$\eth_2^{AF} = \frac{\alpha_2\rho|h_2|^2|h_t|^2}{(\alpha_1 + d_0)\rho|h_2|^2|h_t|^2 + d_1|h_t|^2 + d_2|h_2|^2 + \frac{1}{\rho}} \tag{21}$$

where $d_0 = \kappa_t^2 + \kappa_r^2 + \kappa_t^2\kappa_r^2$ gives the upper bound of $\eth_2$ characterized by the levels of impairment. $d_1 = 1 + \kappa_t^2$ and $d_2 = 1 + \kappa_r^2$ are the aggregate distortion levels at the first and second hops with regard to CR-NOMA. At *U1*, interference in the form of a signal from *U2* can be detected prior to the SIC operation. The corresponding SNDR in this scenario can be represented [55] as

$$\eth_{2\to 1}^{AF} = \frac{\alpha_2 \rho |h_1|^2 |h_t|^2}{(\alpha_1 + d_0)\rho |h_1|^2 |h_t|^2 + d_1 |h_t|^2 + d_2 |h_1|^2 + \frac{1}{\rho}} \tag{22}$$

Hence, the SNDR at *U1* to decode $s_1(t)$ is giving by

$$\eth_1^{AF} = \frac{\alpha_1 \rho |h_1|^2 |h_t|^2}{d_1 |h_t|^2 + \rho d_2 |h_1|^2 + \frac{1}{\rho}} \tag{23}$$

For impSIC plus HWI, (24) provides the SNDR for signal detection to *U1:*

$$\eth_{1,AF}^{impSIC} = \frac{\alpha_1 \rho |h_1|^2 |h_t|^2}{(\alpha_2 + d_0)\zeta \rho |h_1|^2 |h_t|^2 + d_1 |h_t|^2 + d_2 |h_1|^2 + \frac{1}{\rho}}. \tag{24}$$

1) ACHIEVABLE RATE ANALYSIS

From the SINRs and SNDRs analyses, the achievable rates of *U1* and *U2* in bit/s/Hz for each scenario of the system operating with a bandwidth of B and impairment parameters can be expressed as follows:

$$R_2^{AF} = B \log_2 \left(1 + \eth_2^{AF}\right) \tag{25}$$

$$R_1^{AF} = B \log_2 \left(1 + \eth_1^{AF}\right) \tag{26}$$

$$R_{1,AF}^{impSIC} = B \log_2 \left(1 + \eth_{1,AF}^{impSIC}\right) \tag{27}$$

2) OUTAGE PROBABILITY ANALYSIS

(a) Ideal system hardware and SIC: When two users utilize NOMA with varying quality of service (QoS), their respective data rates may require adjustment. The outage performance can be evaluated by setting a threshold target rate, δ_{th_i}, where $\delta_{th_i} = 2^{2\bar{R}_i} - 1$ with $\bar{R}_i$ as the target rate for the ith user. The outage probability of *U2* for detecting $s_2(t)$ is expressed in [55] as:

$$P_2^{AF} = P\left(\begin{matrix}\rho |h_2|^2 \left(\rho |h_t|^2 (\alpha_2 - \alpha_1 \delta_{th_2}) - \delta_{th_2}\right) \\ \leq \delta_{th_2} (\rho |h_t|^2 + 1)\end{matrix}\right). \tag{28}$$

In the event where $|h_t|^2 \leq \frac{\delta_{th_2}}{\rho(\alpha_2 - \alpha_1 \delta_{th_2})}$, $P_2^{AF} = 1$, otherwise, the probability is given by,

$$P_2^{AF} = 1 - \exp\left(-\frac{2\delta_{th_2}}{\rho\left(\alpha_2 - \alpha_1 \delta_{th_2}\right)}\right) \times (\xi) \times K_1(\xi) \tag{29}$$

where $\xi = 2\sqrt{\frac{\delta_{th_2}(\delta_{th_2} + (\alpha_2 - \alpha_1)\delta_{th_2})}{\rho^2(\alpha_2 - \alpha_1 \delta_{th_2})^2}}$, and $K_1(\cdot)$ is Bessel function of the second kind.

The outage probability of *U1* to detect $s_1(t)$ using (18) and (19) is given by

$$P_1^{AF} = P\left(|h_1|^2 < \frac{\rho |h_t|^2 + 1}{\rho(\rho\chi |h_t|^2 - 1)}\right). \tag{30}$$

In a situation where, $\chi \rho |h_t|^2 - 1 < 0$, $P_1^{AF} = 1$, otherwise the probability of *U1* is given by,

$$\begin{aligned} P_1^{AF} &= 1 - P\left(\begin{matrix} \frac{\alpha_2 \rho |h_t|^2 |h_1|^2}{\alpha_1 \rho |h_t|^2 |h_1|^2 + |h_t|^2 + |h_1|^2 + \frac{1}{\rho}} \\ \geq \quad \delta_{th_2}, \ \frac{\alpha_1 \rho |h_t|^2 |h_1|^2}{|h_t|^2 + |h_1| + \frac{1}{\rho}} \geq \delta_{th_1}\end{matrix}\right) \\ &= 1 - 2\exp\left(-\frac{2}{\rho\chi}\right)\sqrt{\frac{1}{\rho^2\chi}\left(\frac{1}{\chi} + 1\right)} \\ &\quad \times K_1\left(2\sqrt{\frac{1}{\rho^2\chi}\left(\frac{1}{\chi} + 1\right)}\right), \end{aligned} \tag{31}$$

where, $\chi \cong \min(\frac{\alpha_2}{\rho^2\chi} - \alpha_1, \frac{\alpha_1}{\delta_{th_1}})$.

(b) Ideal system hardware and impSIC: Here, the outage probability of *U2* for detecting $s_2(t)$ [19], [55], [84], where there is ideal system hardware but impSIC operation is given in (32), shown at the bottom of this page, using (19) and (20). For $\rho^2 \ggg 1$, an approximation of the SINR at *U1* to detect *U2*'s signal as noise can be expressed as:

$$\frac{\alpha_2 \rho |h_t|^2 |h_1|^2}{\alpha_1 \rho |h_t|^2 |h_1|^2 + |h_t|^2 + |h_1|^2 + \frac{1}{\rho}} \approx \frac{\alpha_2}{\alpha_1}, \tag{33}$$

then (32) can be written as,

$$P_{1,AF}^{impSIC} = 1 - \left\{\begin{matrix} P\left(\frac{\alpha_2}{\alpha_1} \geq \delta_{th_2}\right) \\ \times P\left(\begin{matrix}\frac{\alpha_1 \rho |h_t|^2 |h_1|^2}{\rho\zeta^2 + (|h_t|^2 + |h_1|^2) + \frac{1}{\rho}} \\ \geq \delta_{th_1}\end{matrix}\right)\end{matrix}\right\}. \tag{34}$$

Here,

$$P_{1,AF}^{impSIC} = 1, \ \text{if} \ \frac{\alpha_2}{\alpha_1} < \delta_{th_2}. \tag{35}$$

In the case where $\frac{\alpha_2}{\alpha_2} \geq \delta_{th_2}$, (32) becomes

$$P_{1,AF}^{impSIC} = 1 - P\left(|h_1|^2 \geq \frac{\delta_{th_1}\left(\zeta^2\rho + |h_t|^2 + \frac{1}{\rho}\right)}{\alpha_1 \rho |h_t|^2 - \delta_{th_1}}\right), \tag{36}$$

Consider a situation where the denominator is less than zero; that is, $\alpha_1 \rho |h_t|^2 - \rho \delta_{th_1} < 0$, which leads to $|h_t|^2 < \delta_{th_1}/\rho\alpha_1$. In this case, $P_{1,AF}^{impSIC} = 1$. On the other hand, the outage probability is given by

$$P_{1,AF}^{impSIC} = 1 - \exp\left(-\frac{2\delta_{th_1}}{\alpha_1 \rho}\right) \times \phi(a, b) \tag{37}$$

where $\frac{\zeta \delta_{th_1}}{\alpha_1} = a$, $b = \frac{\delta_{th_1}}{\alpha_1 \rho^2}(\frac{\delta_{th_1}}{\alpha_1} + 1)$ and $\phi(a, b) \cong 2\exp(-b/a) \times [a\Gamma(2)/2 \times \exp(a) \times \Gamma(-1, a) - \int_0^b \sqrt{y} \times K_1(2\sqrt{y}) \times \exp(-y/a) dy]$

(c) System with HWI and ideal SIC: When there is a system HWI with a perfect SIC operation, the outage probability of *U2* for detecting $s_2(t)$ [19], [55] can be expressed as

$$P_2^{AF} = P(\eth_2^{AF} < \delta_{th_2}) = 1 - P(\eth_2^{AF} \geq \delta_{th_2}). \quad (38)$$

Substituting (21) into (38), the outage becomes,

$$P_2^{AF} = P\left(|h_2|^2 > \frac{\delta_{th_2}\left(d_1|h_t|^2 + \frac{1}{\rho}\right)}{\left(\rho\alpha_2|h_t|^2 - \delta_{th_2}(\alpha_1 + d_0)|h_t|^2 - \frac{\delta_{th_2}d_2}{\rho}\right)} \right). \quad (39)$$

In the event that $\alpha_2\rho|h_t|^2 - \delta_{th_2}(\alpha_1 + d_0)\rho|h_t|^2 - d_2\delta_{th_2} \leq 0$. In this case, $|h_t|^2 \leq \frac{\delta_{th_2}d_2}{\alpha_2\rho - \rho(\alpha_1+d_0)\delta_{th_2}}$ and the $P_2^{AF} = 1$; otherwise, the outage is given by

$$P_2^{AF} = 1 - \exp\left(-\frac{\delta_{th_2}(d_1 + d_2)}{\rho\left(\alpha_2 - (\alpha_1 + d_0)\delta_{th_2}\right)}\right) \times \psi \times K_1(\psi_1), \quad (40)$$

where $\psi_1 = 2\sqrt{\frac{\delta_{th_2}(d_1d_2\delta_{th_2} + \alpha_2 - (\alpha_1+d_0)\delta_{th_2})}{\rho^2(\alpha_2 - \alpha_1\delta_{th_2}d_0)^2}}$.

The outage probability of *U1* detecting its signal $s_1(t)$ in a system with HWI is given by

$$P_1^{AF} = P\left(|h_1|^2 < \frac{d_1\rho\,|h_t|^2 + 1}{\rho(\chi\rho\,|h_t|^2 - d_2)}\right), \quad (41)$$

where $\chi \cong \min\left(\frac{\alpha_2}{\delta_{th_2}} - (\alpha_1 + d_0), \frac{\alpha_1}{\delta_{th_1}}\right)$. $P_1^{AF} = 1$ for $\chi\rho|h_t|^2 - d_2 < 0$. When $\chi\rho|h_t|^2 - d_2 \geq 0$, the outage becomes

$$P_1^{AF} = 1 - \exp\left(-\frac{d_1 + d_2}{\rho\chi}\right) \times \psi_2 \times K_1(\psi_2), \quad (42)$$

where $\psi_2 = 2\sqrt{\frac{1}{\rho^2\chi}\left(\frac{d_1d_2}{\chi} + 1\right)}$.

(d) System with HWI and impSIC: The outage probability of *U1* when there are imperfections in the system is given by

$$P_1{}^{AF} = 1 - \exp\left(-\frac{\delta_{th_1}(d_2 + d_1)}{\alpha_1\rho}\right) \times \phi(c, d), \quad (43)$$

where $c \cong \frac{\zeta\delta_{th_1}}{\alpha_1}$, $d \cong \frac{\delta_{th_1}}{\alpha_1\rho^2}(\frac{d_2\delta_{th_1}}{\alpha_1} + 1)$, and $\phi(c, d) \cong 2\exp(-d/c) \times [c\Gamma(2)/2 \times \exp(c) \times \Gamma(-1, c) - \int_0^d \sqrt{y} \times K_1(2\sqrt{y}) \times \exp(-y/c)dy]$.

3) BER ANALYSIS

The bit-error analysis for the proposed CR-NOMA system was performed in accordance with the guidelines in [84], [85]. The average error probability (P_e^{U1}) [84] for *U1* when its symbols are correctly and incorrectly identified via SIC processing can be expressed as [84] is expressed as,

$$P_e^{\mathrm{U1}} = \frac{1}{2}\left(1 - \sqrt{\frac{\gamma_{\mathcal{B}_1}}{2 + \gamma_{\mathcal{B}_1}}}\right) + \frac{1}{8}\left[\sqrt{\frac{\gamma_{\mathcal{B}_2}}{2+\gamma_{\mathcal{B}_2}}} - \sqrt{\frac{\gamma_{\mathcal{B}_3}}{2+\gamma_{\mathcal{B}_3}}} + \sqrt{\frac{\gamma_{\mathcal{B}_4}}{2+\gamma_{\mathcal{B}_4}}} - \sqrt{\frac{\gamma_{\mathcal{B}_5}}{2+\gamma_{\mathcal{B}_5}}}\right], \quad (44)$$

where ε_1 and ε_2 are the *U1* and *U2* signal energies, respectively. The SNRs of different constellation points of $s_1(t)$ and $s_2(t)$ are given by

$$\gamma_{\mathcal{B}_1} = \frac{\varepsilon_1}{N_0}\mathbb{E}\left[\left|h_{R,1}\right|^2\right],$$
$$\gamma_{\mathcal{B}_2} = \frac{\left(\sqrt{2\varepsilon_2} + \sqrt{\varepsilon_1}\right)^2}{N_0}\mathbb{E}\left[\left|h_{R,1}\right|^2\right],$$
$$\gamma_{\mathcal{B}_3} = \frac{\left(\sqrt{2\varepsilon_2} - \sqrt{\varepsilon_1}\right)^2}{N_0}\mathbb{E}\left[\left|h_{R,1}\right|^2\right], \quad (45)$$

and

$$\gamma_{\mathcal{B}_4} = \frac{\left(2\sqrt{2\varepsilon_2} + \sqrt{\varepsilon_1}\right)^2}{N_0}\mathbb{E}\left[\left|h_{R,1}\right|^2\right],$$
$$\gamma_{\mathcal{B}_5} = \frac{\left(2\sqrt{2\varepsilon_2} - \sqrt{\varepsilon_1}\right)^2}{N_0}\mathbb{E}\left[\left|h_{R,1}\right|^2\right]. \quad (46)$$

Equation (45) represents the condition under which *U1* can correctly detect its signals, whereas (46) represents the condition under which the signals are incorrectly detected.

Similarly, the total average BER (P_e^{U2}) performance of *U2* from [84] is

$$P_e^{\mathrm{U2}} = \frac{1}{4}\left[\left(1 - \sqrt{\frac{\gamma_{\mathcal{A}_1}}{2 + \gamma_{\mathcal{A}_1}}}\right) + \left(1 - \sqrt{\frac{\gamma_{\mathcal{A}_2}}{2 + \gamma_{\mathcal{A}_2}}}\right)\right]. \quad (47)$$

From (47), $\gamma_{\mathcal{A}_1}$ and $\gamma_{\mathcal{A}_2}$ are the SNRs of the different signal constellation points, which can be expressed as

$$\gamma_{\mathcal{A}_1} = \frac{\left(\sqrt{2\varepsilon_2} + \sqrt{\varepsilon_1}\right)^2}{N_0}\mathbb{E}\left[\left|h_{R,2}\right|^2\right]$$
$$\gamma_{\mathcal{A}_2} = \frac{\left(\sqrt{2\varepsilon_2} - \sqrt{\varepsilon_1}\right)^2}{N_0}\mathbb{E}\left[\left|h_{R,2}\right|^2\right]. \quad (48)$$

B. APPLICATION OF DF CODING SCHEME

1) ACHIEVABLE RATE ANALYSIS

Similar to the AF coding scheme analysis, an achievable rate analysis was performed following the work in [19], [55]. According to NOMA concept, the relay first decodes the signal of *U2* ($s_2(t)$) by invoking SIC, and $s_1(t)$ is decoded later. Therefore, the received SNDRs of $s_1(t)$ and $s_2(t)$ at the relay

$$P_{1,AF}^{impSIC} = 1 - P\left(\frac{\alpha_2\rho|h_t|^2|h_1|^2}{\rho\alpha_1|h_t|^2|h_1|^2 + |h_t|^2 + |h_1|^2 + \frac{1}{\rho}} \geq \delta_{th_2}, \frac{\alpha_1\rho|h_t|^2|h_1|^2}{\rho\zeta^2 + |h_t|^2 + |h_1|^2 + \frac{1}{\rho}} \geq \delta_{th_1}\right) \quad (32)$$

are given by

$$\eth_2^{DF} = \frac{\alpha_2 \rho P_s |h_t|^2}{\alpha_1 \rho P_s |h_t|^2 + \rho |h_t|^2 P_s \kappa_t^2 + 1} \tag{49}$$

and

$$\eth_1^{DF} = \frac{\alpha_1 \rho P_s |h_t|^2}{\alpha_2 \rho P_s |h_t|^2 + \rho |h_t|^2 P_s \kappa_t^2 + 1}. \tag{50}$$

After decoding and encoding, the relay forwards the signal to the all users. Thus, the received SINR at *U2* is expressed as

$$\varsigma_2^{DF} = \frac{\alpha_2 P_r \rho |h_2|^2}{\rho \alpha_1 P_r |h_2|^2 + \rho |h_2|^2 P_r \kappa_r^2 + 1}. \tag{51}$$

Similarly, the SINRs for *U1* [19] are given by

$$\varsigma_{1,DF}^{impSIC} = \frac{\alpha_1 P_r \rho |h_1|^2}{\rho \zeta \alpha_2 P_r |h_1|^2 + \rho |h_1|^2 P_r \kappa_r^2 + 1} \tag{52}$$

and

$$\varsigma_{2\to 1}^{DF} = \frac{\alpha_2 |h_1|^2 \rho P_r}{\alpha_1 |h_1|^2 \rho P_r + |h_1|^2 \kappa_r^2 \rho + 1}. \tag{53}$$

From (51) and (52), the achievable rates can be expressed as

$$R_2^{DF} = B \log_2 \left(1 + \eth_2^{DF}\right) \tag{54}$$

$$R_1^{DF} = B \log_2 \left(1 + \frac{\alpha_1 |h_2|^2 \rho'}{\alpha_2 \kappa_r^2 |h_1|^2 \rho' + 1}\right) \tag{55}$$

$$R_{1,DF}^{impSIC} = B \log_2 \left(1 + \eth_{1,DF}^{impSIC}\right) \tag{56}$$

2) OUTAGE PROBABILITY

The probability of an outage metric evaluates the likelihood that a communication channel is unable to maintain a specific information rate owing to variations in channel capacity. This is calculated based on the probability that the channel capacity will fall below the minimum required rate. Various factors can influence outage probability, such as the SNR, fading channel coefficient, co-channel interference, and diversity-combining schemes used in wireless communication systems. Under the DF coding scheme, the outage probability and BER of the system with HWI and impSIC are given below, following the analysis in [55].

(a) System with ideal hardware and SIC: The outage probability of the system without the impairment parameter under the DF coding scheme is analyzed below. The outage probability of $s_1(t)$ at *U1* is given by

$$P_1^{DF} = 1 - \exp\left(-\frac{\Omega_1}{|h_1|^2}\right), \tag{57}$$

where $\Omega_1 = \max(\frac{\delta_{th_2}}{\alpha_2 \rho - \delta_{th_2} \rho \alpha_1}, \frac{\delta_{th_1}}{\alpha_1 \rho})$. The probability of an outage in detecting $_2(t)$ at

$$P_2^{DF} = 1 - \exp\left(-\frac{\delta_{th_2}}{|h_2|^2 \rho \left(\alpha_2 \rho - \alpha_1 \rho \delta_{th_2}\right)}\right). \tag{58}$$

(b) System with ideal hardware and impSIC: Here, only the outage probability of detecting $s_1(t)$ at *U1* is considered because the SIC operation is performed at *U1*. The outage probability is given by:

$$\begin{aligned} P_{1,DF}^{impSIC} &= 1 - |h_1|^2 \exp\left(-\frac{1}{|h_1|^2}\right) \\ &\quad + \left(\frac{\alpha_1}{\varepsilon^2 \zeta |h_2|^2 \delta_{th_1}} + \frac{1}{|h_1|^2}\right)^{-1} \exp\left(\frac{1}{\varepsilon^2 \rho \zeta |h_2|^2}\right) \\ &\quad \times \exp\left(-\left(\frac{\alpha_1}{\varepsilon^2 \zeta |h_2|^2 \delta_{th_1}} + \frac{1}{\varepsilon^2 |h_2|^2}\right)\right), \end{aligned} \tag{59}$$

where ε^2 is a system parameter.

(c) System with HWI and ideal SIC: In a situation where the system has only HWI, the outage probability of detecting $s_1(t)$ at *U1* is:

$$P_1^{DF} = 1 - \exp\left(-\frac{\Omega_2}{|h_1|^2}\right), \tag{60}$$

where $\Omega_2 = \max\left(\frac{\delta_{th_2}}{\alpha_2 \rho - \delta_{th_2} \rho (\alpha_1 + d_0)}, \frac{\delta_{th_1}}{\zeta \rho}\right)$.

Similarly, the outage probability for detecting $s_2(t)$ at *U2* is given by

$$P_2^{DF} = 1 - \exp\left(-\frac{\delta_{th_2}}{\alpha_2 \rho |h_2|^2 - \delta_{th_2} |h_2|^2 \rho (p1 + d_0)}\right). \tag{61}$$

(d) System with HWI and impSIC: From the definition, the outage probability of the users can be expressed as

$$P_i = 1 - \left(1 - P_{s_i}^t\right)\left(1 - P_{s_i}^{r,i}\right), \quad i = 1, 2 \tag{62}$$

where for $i = 1$, $j = t$, (1), and

$$\begin{aligned} P_{s_1}^j &= P\left(\hbar_2^j \le \delta_{th_2}\right) + p\left(\hbar_2^j > \delta_{th_2}\right) P\left(\hbar_2^j \le \delta_{th_1}\right) \\ &= 1 - \exp\left(-\tau_2^j \delta_{th_2}\right) \exp\left(-\tau_1^j \delta_{th_1}\right), \end{aligned} \tag{63}$$

where

$$\begin{aligned} &\hbar_1^t = \varsigma_1^{DF},\ \hbar_1^1 = \eth_{1,DF}^{impSIC} \\ &\tau_2^t = \frac{\left(\frac{N_0}{2} + \sigma_\in^2 P_s + \sigma_\in^2 P_s \kappa_t^2\right)}{\Upsilon_t \left(\alpha_2 P_s - \delta_{th_2} P_s \alpha_2 - \delta_{th_2} P_s \kappa_t^2\right)} \\ &\tau_2^1 = \frac{\left(\frac{N_0}{2} + \sigma_\in^2 P_r + \sigma_\in^2 P_r \kappa_t^2\right)}{\Upsilon_1 \left(\alpha_2 P_r - \delta_{th_2} P_s \alpha_1 - \delta_{th_2} P_r \kappa_r^2\right)} \\ &\tau_1^1 = \frac{\left(\frac{N_0}{2} + \sigma_\in^2 P_r + \sigma_\in^2 P_r \kappa_r^2\right)}{\Upsilon_1 \left(\alpha_1 P_r - \delta_{th_1} \zeta P_r \alpha_2 - \delta_{th_1} P_s \kappa_r^2\right)} \\ &\Upsilon_j = E\left[\left|h_j\right|^2\right] \\ &\delta_{th_2} = 2^{2R_2} - 1. \end{aligned} \tag{64}$$

For $i = 2$ and $j = t,\ 2$

$$P_{s_2}^{j} = P\left(\hbar_2^{j} \leq \delta_{th_2}\right) = 1 - \exp\left(-\delta_{th_2}\tau_2^{j}\right) \tag{65}$$

where

$$\begin{aligned}
\hbar_2^{t} &= \varsigma_2^{DF},\ \hbar_2^{2} = \eth_2,\\
\tau_1^{t} &= \frac{\left(\frac{N_0}{2} + \sigma_{\in}^2 P_s + \sigma_{\in}^2 P_s \kappa_t^2\right)}{\Upsilon_t\left(\alpha_1 P_s - \zeta\delta_{th_1} P_s \alpha_2 - \delta_{th_1} P_s \kappa_r^2\right)},\\
\delta_{th_1} &= 2^{2R_1} - 1,\\
\tau_1^{2} &= \frac{\left(\frac{N_0}{2} + \sigma_{\in}^2 P_r + \sigma_{\in}^2 P_r \kappa_r^2\right)}{\Upsilon_1\left(\alpha_2 P_r - \delta_{th_2} P_r \alpha_1 - \delta_{th_2} P_s \kappa_r^2\right)},\\
\Upsilon_i &= E\left[|h_i|^2\right].
\end{aligned} \tag{66}$$

3) BER ANALYSIS

Considering binary phase-shift keying modulation technique, the BER at the relay and destination of the ith user for $i = \{1,\ 2\}$ is given by

$$P_i^{error} = P_{m_i,t}\left(1 - P_{m_i,(r,i)}\right) + \left(1 - P_{m_i,t}\right) P_{m_i,(ri)}, \tag{67}$$

where $P_{m_i,(t)}$ is the BER of *U1* and *U2* symbols in the first phase and, $P_{m_i,(r,i)}$ is the BER of *U1* and *U2* in the second phase. The BER for detecting $s_2(t)$ symbols in the presence of HWI and impSIC is given by:

$$P_{s_2,j} = \frac{1}{2}\sum_{z=1}^{2} Q\left(\sqrt{2\delta_{s_2,j,z}}\right);\quad j = \{t,\ 2\}, \tag{68}$$

where for

$$\begin{aligned}
\delta_{s_2,j,z} &= \frac{P_{s|r}\varpi_z\left|h_j\right|^2}{N_0 + 2P_{s|r}\kappa_j^2\left|h_j\right|^2 + 2\left(\kappa_j^2 + \varpi_z\right)P_{s|r}\sigma_{\in}^2},\\
\varpi_z &= \left[\left(\sqrt{\alpha_1} + \sqrt{\alpha_2}\right)^2, \left(\sqrt{\alpha_2} - \sqrt{\alpha_1}\right)^2\right].
\end{aligned} \tag{69}$$

The average BER of $s_2(t)$ in the first time slot by the relay and the second time slot by $U2$ is given by:

$$P_{s_2,j}^{DF} = \frac{1}{4}\sum_{z=1}^{2}\left(1 - \sqrt{2\bar{\delta}_{s_2,j,z}}\right);\quad j = \{t,\ 2\}. \tag{70}$$

where $\bar{\delta}_{s_2,j,z} = E[|\delta_{s_2,j,z}|]$.

U1 performs SIC to detect $s_1(t)$ symbols. The BER for detecting $s_1(t)$ is the sum of the correct and incorrect detections of $s_2(t)$ during the SIC operation. When both HWI and impSIC are present at the relay and U1, the BER of s1(t) is

$$P_{s_1,j}^{DF} = \frac{1}{2}\sum_{z=1}^{6} g_z Q\left(\sqrt{2\delta_{s_1,j,z}}\right);\quad j = \{t,\ 1\}, \tag{71}$$

where

$$g_z = [1, 1, -1, 1, 1, -1] \qquad \text{and}$$

TABLE 3. Simulation Settings

Parameters	Values
Operating frequency	2.6 GHz
$\theta_{tilt},\ \theta_{3dB},\ \phi_{3dB}$	$95^\circ,\ 15^\circ,\ 70^\circ$
Operating bandwidth	200 MHz
Antenna configuration	CA
Hardware impairment or distortion factor	0.15
Channel estimation error & Imperfect SIC factor	0.02
Channel model	Three-dimension GBSM
Environment	Urban macrocell
Target rate $(R_1,\ R_2)$	(0.5, 0.1) b/s/Hz
Fixed power allocation	User1 (*U1*), $\alpha_1 = 0.2$ User2 (*U2*), $\alpha_2 = 0.8$

$$\delta_{s_1,j,z} = \frac{P_{s|r}\varsigma_z\varpi_z\left|h_j\right|^2}{N_0 + 2P_{s|r}\kappa_j^2\left|h_j\right|^2 + 2\left(\kappa_j^2 + \varpi_z\right)P_{s|r}\sigma_{\in}^2} \tag{72}$$

Here, the modulation of $s_1(t)$ is given by,

$$\psi_z = \begin{bmatrix} \left(\sqrt{\alpha_1} + \sqrt{\alpha_2}\right)^2, \left(\sqrt{\alpha_2} - \sqrt{\alpha_1}\right)^2, \left(\sqrt{\alpha_1} + \sqrt{\alpha_2}\right)^2, \\ \left(\sqrt{\alpha_1} + \sqrt{\alpha_2}\right)^2, \left(\sqrt{\alpha_2} - \sqrt{\alpha_1}\right)^2, \left(\sqrt{\alpha_2} - \sqrt{\alpha_1}\right)^2 \end{bmatrix} \tag{73}$$

The SIC condition for detecting both correct and incorrect symbols is ς_z. In an incorrect SIC operation, the $s_2(t)$ symbols subtracted from the received signal are erroneously detected, thereby shifting the detection rule. The average BER of $s_1(t)$ can be expressed by applying the moment-generating function and an alternative form of the $Q(\cdot)$ function:

$$P_{s_1,j}^{DF} = \frac{1}{4}\sum_{z=1}^{6} g_z\left(1 - \sqrt{2\bar{\delta}_{s_1,j,z}}\right);\quad j = \{t,\ 1\}. \tag{74}$$

IV. NUMERICAL RESULTS AND DISCUSSIONS

In this section, the performance of the proposed GBSM-based CR-NOMA system with HWI and impSIC is evaluated through numerical analysis. Using Algorithm 1, antenna position vectors that are essential for determining the array response were created. Subsequently, all simulations were carried out utilizing the Monte Carlo method. In this research, the BER, achievable rates, and outage probability were compared to those of a similar system that does not consider impairment characteristics. Table 3 presents the simulation settings for the analysis of the proposed system. These settings include parameters for the impSIC, channel estimation error, and HWI factor, which are the most significant distortion factors according to the previous literature. These distortions have a significant impact on the system performance. Table 3 lists the data or target rates for different users based on their channel conditions. Consequently, NU had a higher rate than FU. This difference is due to the fact that the squared magnitude of the

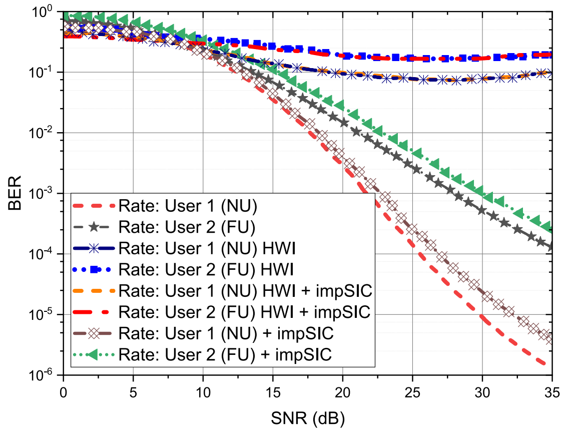

FIGURE 4. BER performance of the proposed system under various impairment scenarios using the AF coding scheme.

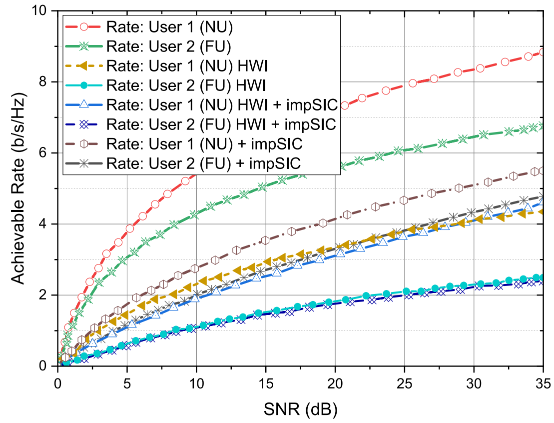

FIGURE 6. Achievable rate performance of the proposed system under various impairment scenarios using the AF coding scheme.

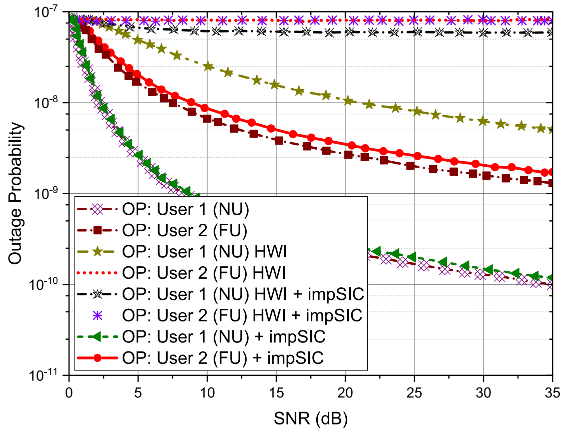

FIGURE 5. Outage probability performance of the proposed system under various impairment scenarios using the AF coding scheme.

channel coefficient for the NU is always larger than that of the FU. This ensures that users experience no outages, leading to an uninterrupted data transmission.

A. PERFORMANCE OF AF CODING SCHEME

The simulation results are plotted in Figs. 4, 5, and 6 and were obtained by modeling the transmitting antenna as a CA.

1) BER PERFORMANCE

The simulation results of the CR-NOMA system are shown in Fig. 4. It shows the BER in relation to the SNR under different operating conditions, such as perfect hardware and SIC, HWI only, impSIC only, and both HWI and impSIC. HWI significantly degraded performance, causing distortion in each phase as the signal passed through the relay. All the users receive a distorted signal. The system's HWI and SIC operational imperfections primarily cause these distortions. The presence of both HWI and impSIC degrades the BER performance of all users compared with a system without these imperfections. When employing perfect hardware and SIC, the BER for both users demonstrated a monotonically increasing trend as the SNR increased, serving as a lower bound on achievable performance. This observation aligns with the fundamental principles of wireless communication, in which a higher SNR typically leads to a lower BER. According to the AF BER analysis results for different impairment scenarios, all possibilities up to a 15 dB SNR seem equivalent. This proves that if the SNR is just maintained below 15 dB, then both NU and FU can experience equivalent performance.

At an SNR of 10 dB with perfect hardware and SIC, the BERs were approximately $10^{-0.85}$ for the FU and $10^{-0.90}$ for the NU. At a high SNR of 20 dB, the perfect case BERs improved to $10^{-1.93}$ for FU and $10^{-2.80}$ for NU. The implementation of HWI significantly degrades the BER only across the SNR range, particularly at high SNR values. The degradation in BER performance is approximately $10^{-0.90}$ for FU and $10^{-1.10}$ for NU. BER degradation is reasonably constant across SNRs, indicating that the effect of impSIC errors is independent of SNR. With impSIC only, at an SNR of 10 dB, the BERs were $10^{-0.75}$ for the FU and $10^{-0.9}$ for the NU, indicating a smaller degradation compared to the case in which only HWI was applied. The combination of HWI and impSIC yields the lowest BER. At very high SNRs, the difference between the ideal and actual cases decreased, suggesting a complex relationship between the HWI, impSICs, and SNR. When HWI and impSIC are combined, the BER decreases further, reaching $10^{-0.70}$ for the FU constellation and $10^{-0.83}$ for NU constellation at a 10 dB SNR, respectively. However, at a higher SNR of 20 dB, the BER for the HWI case worsened to $10^{-0.80}$ for the FU and $10^{-1.00}$ for the NU. Notably, the performance gap between the ideal case and the actual case is greater at 20 dB SNR for the HWI compared at 10 dB SNR, indicating that HWI has a more significant impact at higher SNRs.

The performance of NU was consistently superior to that of FU at all SNR values because of the favorable channel conditions. The results indicated that, as the SNR increased, the signal strengthened relative to the interference, making it less likely to experience an outage. Furthermore, the degradation trends caused by HWI and impSIC were consistent for both users, indicating that these factors affected all users in the system regardless of their proximity to the source. The relay amplifies and transmits the composite signal, which includes the interference caused by the NU on the FU, thereby exacerbating the effects of the SIC errors. The BER of the FU is further compromised by two compounding factors: a lower channel gain owing to severe path loss, and residual interference remaining after impSIC.

2) OUTAGE PROBABILITY PERFORMANCE

Similarly, the simulation results of the outage probability performance of a proposed system under various scenarios are presented in Fig. 5. The graph depicted in Fig. 5 was obtained using (29), (37), (40), (42), and (43) in Section III-A of Section IV, which illustrates the relationship between outage probabilities and SNRs for CR-NOMA.

The graph shows the impact of various impairment conditions on the system performance. Perfect hardware and SIC demonstrate superior outage performance for both the NU and FU as the SNR increases, serving as a benchmark for the system's potential. Regarding outage probability, the performances are steady for both the DF and AF impairment scenarios. After 20 dB, under AF, the performances of both users were remarkably consistent. HWI alone significantly decreased the outage probability across all SNRs, especially at high levels, thereby emphasizing the detrimental effects of hardware imperfections. The introduction of impSIC worsens the outage, but with less dependency, as the effect remains relatively constant regardless of the SNR. The combination of HWI and impSIC results in the worst performance. Nevertheless, the gap from the perfect case narrowed at very high SNRs, suggesting complex interplay between these factors.

Across all SNRs, NU consistently outperformed FU owing to superior channel conditions. Notably, the degradation trends caused by HWI and impSIC are similar for both users, implying a generalized impact on the system, regardless of user proximity to the source. Qualitatively, at an SNR of 10 dB, the ideal scenario exhibits outage probabilities of approximately $10^{-8.40}$ and $10^{-9.40}$ for the FU and NU, respectively. The introduction of HWI alone increased these values to approximately $10^{-7.70}$ and $10^{-7.20}$, representing a significant increase in the outage probability, which is nearly an order of magnitude. With impSIC alone, the degradation at the same SNR was smaller, with outage probabilities of $10^{-8.10}$ and $10^{-9.20}$ for FU and NU, respectively.

Combining HWI and impSIC results in further deterioration, pushing the outage probabilities to $10^{-7.20}$ and $10^{-7.35}$ for FU and NU, respectively, at a 10 dB SNR. At a higher SNR of 20 dB, the ideal-case outage probabilities improve to $10^{-8.80}$ and $10^{-9.83}$ for FU and NU, respectively. However, with HWI, the outage probabilities worsened to $10^{-7.20}$ and $10^{-7.95}$, showing a larger gap from the ideal case compared with the 10 dB SNR, highlighting the impact of HWI at higher SNRs. The outage probability decreases as the SNR increases. This is because as the SNR value increases, the signal becomes stronger relative to the interference and is thus less likely to experience an outage.

3) ACHIEVABLE RATE PERFORMANCE

Fig. 6 shows four simulation scenarios have been presented, including perfect hardware and SIC, HWI only, impSIC only, and both HWI and impSIC. The plot was obtained using (25), (26), and (27). The average achievable data rate, which considers both the channel conditions and allocated data rate over a certain period, is influenced by the state of the channel and any remaining HWI in the system.

According to the figure, in the perfect hardware and SIC scenarios, the achievable rates for both users increased steadily with an increase in SNR, providing a performance upper bound. However, with the introduction of HWI and SIC, the rates for both users degraded compared to the perfect case, especially at higher SNRs, demonstrating the detrimental impact of HWI and SIC on CR-NOMA performance. At an SNR of 10 dB, with perfect hardware and SIC, the FU achieves approximately 4.2 bits per second per hertz (b/s/Hz), whereas the NU achieves around 5.5 b/s/Hz.

With HWI and SIC only, the FU rate decreases to about 1.1 b/s/Hz, whereas that of NU reduces to 2.2 b/s/Hz, indicating an average of 3.3 b/s/Hz degradation for both users due to HWI and SIC. When only impSIC is considered, the degradation is less severe than that with HWI and SIC. The gap from the perfect case remains reasonably constant across SNRs, illustrating the effect of impSIC errors. Here, the rates are around 2.0 b/s/Hz for FU and 2.8 b/s/Hz for NU, with a degradation of 2.2 b/s/Hz for FU and 2.3 b/s/Hz for NU. The combination of HWI and impSIC leads to the largest degradation, at 1.0 b/s/Hz and 2.0 b/s/Hz for FU and NU, respectively. At a higher SNR of 20 dB, the degradation due to HWI becomes more severe. The perfect case rates are around 5.8 b/s/Hz for FU and 7.3 b/s/Hz for NU. Considering the HWI case, the rates drop to about 2.0 b/s/Hz for FU and 3.2 b/s/Hz for NU. However, at this SNR, the gap to the perfect case is lower with both HWI and impSIC compared to 10 dB SNR, with rates of approximately 3.2 b/s/Hz for FU and 4.1 b/s/Hz for NU.

The results are consistent with the findings in the existing literature; NU generally achieves higher rates than FU in all scenarios owing to the better channel conditions in CR-NOMA systems.

B. PERFORMANCE OF DF CODING SCHEME

Figs. 7, 8, and 9 compare the proposed system with the DF coding scheme under HWI and impSIC to a system without these issues.

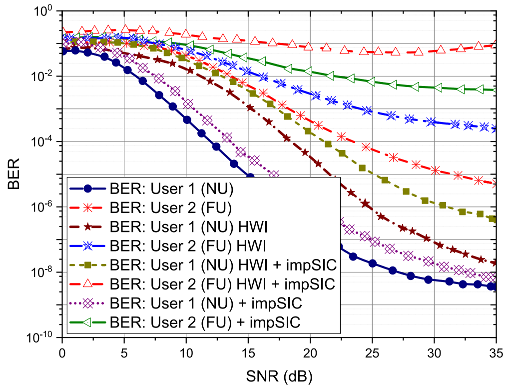

FIGURE 7. BER performance of the proposed system under various impairment scenarios using the DF coding scheme.

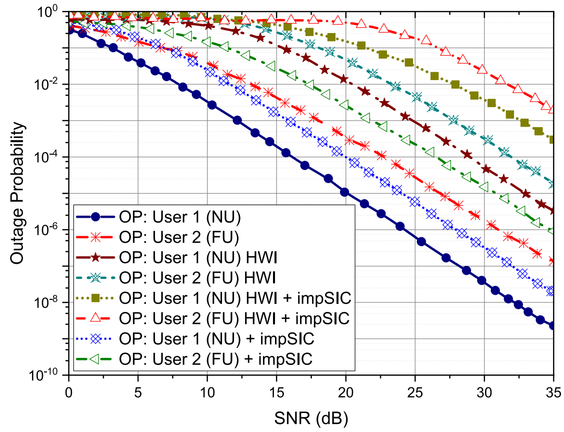

FIGURE 8. Outage probability performance of the proposed system under various impairment scenarios using the DF coding scheme.

1) BER PERFORMANCE

Fig. 7 illustrates the BER performance of the system, which was calculated using equations (70) and (74). The observations made in the DF were similar to those in the AF results. However, SNR must be maintained above 5 dB. While the far user's BER performance starts to improve after 15 dB for AF, things appreciating for DF after 5 dB. Furthermore, analysis reveals that the NU continually exhibits a lower BER across the SNR range owing to more favorable channel conditions. As the SNR increases for both users, the BER decreases, which is a fundamental principle in wireless communication systems, because a higher SNR typically results in lower error rates. At an SNR of 10 dB, with ideal hardware and perfect SIC, the BERs were approximately $10^{-3.60}$ for the NU and $10^{-1.60}$ for FU. However, with HWI and impSICs, BERs were significantly worse than those in the ideal scenario. At 10 dB SNR, the BER of the NU was approximately $10^{-1.80}$, whereas the BER of the FU with impairments was approximately $10^{-0.70}$, representing a substantial increase in the BER compared to the ideal case. From the plot, it can be observed that the difference in BER between the ideal and impaired cases increased as the SNR increased. This trend emphasizes the growing impact of impairments, particularly at higher SNR. Although the BER improves as the SNR increases, practical limitations owing to HWI and impSIC limit the system performance compared to ideal conditions.

2) OUTAGE PROBABILITY PERFORMANCE

The outage probability performance was obtained using (63) and (65). In Fig. 8, at an SNR of 10 dB, without HWI and impSIC, the NU and FU outages were $10^{-2.70}$ and $10^{-1.60}$, respectively. However, the introduction of the HWI alone resulted in a ten-fold increase in outages for both users, with outages increasing to $10^{-0.70}$ for NU and $10^{-0.40}$ for the FU. Notably, the addition of both HWI and impSIC led to an increase in the NU outage to $10^{-0.25}$ and a complete outage for the FU. At an SNR of 20 dB, the outages for NU and FU were both very low at $10^{-5.00}$ and $10^{-3.70}$, respectively, when HWI and impSIC were not used. However, when HWI was used alone, the outages for NU and FU increased to $10^{-2.00}$ and $10^{-1.60}$, respectively. When both HWI and impSIC were used, the NU outage increased to $10^{-0.80}$, whereas the FU outage was complete, indicating that reliable signal decoding was impossible even at higher SNRs. This complete FU loss is particularly interesting because it occurs at a high SNR of 20 dB. This shows that the hardware distortions and interference after impSIC were too strong for FU, making it impossible to decode signals reliably.

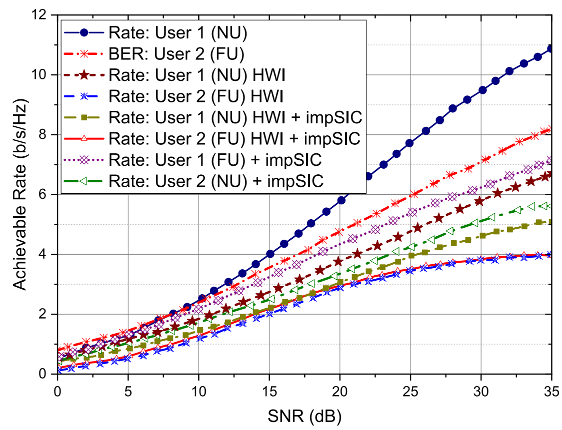

FIGURE 9. Achievable rate performance of the proposed system under various impairment scenarios using the DF coding scheme.

3) ACHIEVABLE RATE PERFORMANCE

Fig. 9 shows the achievable rates for the FU and NU under different conditions. The results were obtained using the expressions in (54), (55) and (56). Without any impairments, the NU achieves a higher rate than the FU across all SNRs because of its more favorable channel conditions. With HWI only, the rates for both users decreased across all SNRs compared to the perfect hardware case. For example, at an SNR of 10 dB, the FU rate decreases from approximately 1.8 b/s/Hz to 1.2 b/s/Hz. This is expected because HWI, such as phase noise and I/Q imbalance, degrade the received signal quality.

TABLE 4. Performance Comparison of CR-NOMA With Impairment in Different Channel Models at 25 dB

Ref.	Coding Scheme	Antenna Type	Channel Model	Transmission Mode	Average Performance			
					BER	outage probability	Throughput (bps)	Rate (b/s/Hz)
[19]	AF	Single antenna	Nakagami-m (CBSM)	Downlink	$10^{-1.18}$	$10^{-1.45}$	-	-
[21]	DF	Single antenna	Rayleigh (CBSM)	Downlink	-	$10^{-1.35}$	3.8	-
[53]	DF	Single antenna	Rayleigh (CBSM)	Downlink	-	-	-	1.72
[55]	AF	Single antenaa	Rayleigh (CBSM)	Downlink	-	$10^{-1.85}$	7.5	-
	DF				-	$10^{-2.80}$	-	-
[33]	DF with MBM	ULA at the BS, single antenna relay & user devices	Rayleigh (CBSM)	Uplink	$10^{-3.75}$	-	-	-
[61]	DF	Single antenna	Rayleigh (CBSM)	Downlink	$10^{-1.16}$	$10^{-1.45}$	-	-
Proposed work	AF	Cylindrical antenna array (CA)	3D GBSM	Downlink	$10^{-1.05}$	$10^{-7.05}$	-	2.90
	DF				$10^{-2.25}$	$10^{-1.23}$	-	5.25

Adding impSIC further reduces the achievable rates, especially for the NU. At 20 dB SNR, the NU rate decreased by 2.0 b/s/Hz compared to HWI only. This indicates that impSIC errors limit NU performance because some FU interference remains after cancellation. The impact of impairments is more pronounced at higher SNRs, as interference and distortion, rather than noise, become limiting factors. For instance, at an SNR of 30 dB with HWI and impSIC, the FU rates plateaued at approximately 4.0 b/s/Hz. When both FU and NU employ impSIC, their rates improve with impSIC only at NU. This demonstrates the benefits of SIC for both receivers in mitigating multiuser interference. The FU rate approached perfect SIC results. Finally, compared with the AF results, after 20 dB, the smallest performance difference was noted for DF.

Table 4 shows the performance of CR-NOMA systems with impairments in different channel models at an SNR of 25 dB. From the table, for both HWI and impSIC, the proposed method achieved a BER of $10^{-1.05}$ and an outage probability of $10^{-7.05}$ for the AF mode, whereas for the DF mode, the BER was $10^{-2.25}$ and the outage probability was $10^{-1.23}$. In terms of AF transmission, the proposed method achieved better error performance and improved reliability with a lower probability of an outage. Nonetheless, the results of this study demonstrate substantial improvements in performance, suggesting that the combination of AF or DF coding schemes in a 3D GBSM with CA could offer significant benefits for CR-NOMA systems.

V. CONCLUSION

In this study, the performance of a GBSM-based CR-NOMA DL system was evaluated in the presence of realistic system impairment parameters. In this study, both AF and DF relay coding schemes, incorporated a CA model for the transmitting antenna and simplified the GBSM channel model by estimating the location vector of the array element based on the array's physical dimensions. The research findings provide valuable insights into the impact of system impairments on two NOMA users. By comparing the BER, achievable rate, and outage probabilities of users in systems with and without impairments, this study demonstrated that all users are affected by impairments, with one user experiencing a more significant impact. Furthermore, this study highlights that systems with impairments amplify performance differences between NU and FU, emphasizing the need for strategies to mitigate the effects of practical system impairments. These findings underscore the need for strategies to mitigate these impairments to ensure fairness and maintain the quality of service. Future research could explore the integration of IRS into GBSM-based LAT systems.

ACKNOWLEDGMENT

The authors are grateful to the Wireless Communication Lab and the Virtual Infosec Lab at the Kwame Nkrumah University of Science and Technology, Ghana, for their support.

REFERENCES

[1] Z. Ding, X. Lei, G. K. Karagiannidis, R. Schober, J. Yuan, and V. K. Bhargava, "A survey on non-orthogonal multiple access for 5G networks: Research challenges and future trends," *IEEE J. Sel. Areas Commun.*, vol. 35, no. 10, pp. 2181–2195, Oct. 2017.

[2] Y. Saito, Y. Kishiyama, A. Benjebbour, T. Nakamura, A. Li, and K. Higuchi, "Non-orthogonal multiple access (NOMA) for cellular future radio access," in *Proc. IEEE 77th Veh. Technol. Conf.*, 2013, pp. 1–5.

[3] K. Higuchi and A. Benjebbour, "Non-orthogonal multiple access (NOMA) with successive interference cancellation for future radio access," *IEICE Trans. Commun.*, vol. 98, no. 3, pp. 403–414, 2015.

[4] X. Pei, Y. Chen, M. Wen, H. Yu, E. Panayirci, and H. V. Poor, "Next-generation multiple access based on NOMA with power level modulation," *IEEE J. Sel. Areas Commun.*, vol. 40, no. 4, pp. 1072–1083, Apr. 2022.
[5] V. Balyan, "Cooperative relay to relay communication using NOMA for energy efficient wireless communication," *Telecommun. Syst.*, vol. 77, no. 2, pp. 271–281, 2021.
[6] J. Ju, G. Zhang, Q. Sun, L. Jin, and W. Duan, "On the performance of receiver strategies for cooperative relaying cellular networks with NOMA," *EURASIP J. Wireless Commun. Netw.*, vol. 2019, no. 1, pp. 1–14, 2019.
[7] Y. Zhou and Y. Chen, "Performance analysis of end-to-end SNR estimators for AF relaying," *Telecommun. Syst.*, vol. 67, pp. 269–280, 2018.
[8] J. Tong and C. Zhong, "Full-duplex two-way AF relaying systems with imperfect interference cancellation in Nakagami-m fading channels," *Sci. China Inf. Sci.s*, vol. 64, no. 8, 2021, Art. no. 182310.
[9] S. Lee, J. Youn, and B. C. Jung, "Hybrid AF/DF cooperative relaying technique with phase steering for industrial IoT networks," *Energies*, vol. 14, no. 4, 2021, Art. no. 937.
[10] M. H. Chinaei, M. J. Omidi, J. Kazemi, and F. S. Tabataba, "Energy efficiency optimization of one-way and two-way DF relaying considering circuit power," *Wireless Netw.*, vol. 22, pp. 367–381, 2016.
[11] F.-X. Socheleau, M. Stojanovic, C. Laot, and J.-M. Passerieux, "Information-theoretic analysis of underwater acoustic OFDM systems in highly dispersive channels," *J. Elect. Comput. Eng.*, vol. 2012, no. 1, 2012, Art. no. 716720.
[12] J. Zhu, Z. Wan, L. Dai, M. Debbah, and H. V. Poor, "Electromagnetic information theory: Fundamentals, modeling, applications, and open problems," *IEEE Wireless Commun.*, vol. 31, no. 3, pp. 156–162, Jun. 2024.
[13] L. Lu, G. Y. Li, A. L. Swindlehurst, A. Ashikhmin, and R. Zhang, "An overview of massive MIMO: Benefits and challenges," *IEEE J. Sel. Topics Signal Process.*, vol. 8, no. 5, pp. 742–758, Oct. 2014.
[14] E. Björnson et al., "Massive MIMO networks: Spectral, energy, and hardware efficiency," *Found. Trends Signal Process.*, vol. 11, no. 3/4, pp. 154–655, 2017.
[15] E. G. Larsson, O. Edfors, F. Tufvesson, and T. L. Marzetta, "Massive MIMO for next generation wireless systems," *IEEE Commun. Mag.*, vol. 52, no. 2, pp. 186–195, Feb. 2014.
[16] W. Tarneberg, M. Karaca, A. Robertsson, F. Tufvesson, and M. Kihl, "Utilizing massive MIMO for the tactile internet: Advantages and tradeoffs," in *Proc. IEEE Int. Conf. Sens., Commun. Netw. Workshops*, 2017, pp. 1–6.
[17] S. A. Khwandah, J. P. Cosmas, P. I. Lazaridis, Z. D. Zaharis, and I. P. Chochliouros, "Massive MIMO systems for 5G communications," *Wireless Pers. Commun.*, vol. 120, no. 3, pp. 2101–2115, 2021.
[18] J. Hoydis, S. Ten Brink, and M. Debbah, "Massive MIMO: How many antennas do we need?," in *Proc. IEEE 49th Annu. Allerton Conf. Commun., Control, Comput.*, 2011, pp. 545–550.
[19] S. Beddiaf et al., "A unified performance analysis of cooperative NOMA with practical constraints: Hardware impairment, imperfect sic and CSI," *IEEE Access*, vol. 10, pp. 132931–132948, 2022.
[20] X. Li, J. Li, Y. Liu, Z. Ding, and A. Nallanathan, "Residual transceiver hardware impairments on cooperative NOMA networks," *IEEE Trans. Wireless Commun.*, vol. 19, no. 1, pp. 680–695, Jan. 2020.
[21] S. Arzykulov, G. Nauryzbayev, A. Celik, and A. M. Eltawil, "Hardware and interference limited cooperative CR-NOMA networks under imperfect SiC and CSI," *IEEE Open J. Commun. Soc.*, vol. 2, pp. 1473–1485, 2021.
[22] F. Harris, "Digital signal processing in radio receivers and transmitters," *Int. J. Wireless Inf. Netw.*, vol. 5, no. 2, pp. 133–145, 1998.
[23] X. Zhang, M. Matthaiou, E. Björnson, M. Coldrey, and M. Debbah, "On the MIMO capacity with residual transceiver hardware impairments," in *Proc. IEEE Int. Conf. Commun.*, 2014, pp. 5299–5305.
[24] A. C. Galetto, J. I. Bonetti, B. T. Reyes, D. A. Morero, and M. R. Hueda, "Digital background compensation of analog impairments in jointly frequency-time interleaved DACs," *IEEE Access*, vol. 11, pp. 96143–96157, 2023.
[25] X. Zhang, M. Matthaiou, M. Coldrey, and E. Björnson, "Impact of residual transmit RF impairments on training-based MIMO systems," *IEEE Trans. Commun.*, vol. 63, no. 8, pp. 2899–2911, Aug. 2015.
[26] Q. Chen, M. Li, X. Yang, R. Alturki, M. D. Alshehri, and F. Khan, "Impact of residual hardware impairment on the IoT secrecy performance of RIS-assisted NOMA networks," *IEEE Access*, vol. 9, pp. 42583–42592, 2021.
[27] J. Bian, C.-X. Wang, X. Gao, X. You, and M. Zhang, "A general 3D non-stationary wireless channel model for 5G and beyond," *IEEE Trans. Wireless Commun.*, vol. 20, no. 5, pp. 3211–3224, May 2021.
[28] W. Zhang, L. Gu, K. Zhang, Y. Zhang, S. Wang, and Z. Ji, "A wideband non-stationary 3D GBSM for hap-MIMO communication systems at millimeter-Wave bands," *Electronics*, vol. 13, no. 4, 2024, Art. no. 678.
[29] G. Sun, R. He, Z. Ma, B. Ai, and Z. Zhong, "A 3D geometry-based non-stationary MIMO channel model for RIS-assisted communications," in *Proc. IEEE 94th Veh. Technol. Conf.*, 2021, pp. 1–5.
[30] Z. Li, H. Chang, J. Huang, and C.-X. Wang, "A general 3D GBSM for 6G satellite communication systems," in *Proc. IEEE/CIC Int. Conf. Commun. China*, 2023, pp. 1–6.
[31] S. Tweneboah-Koduah et al., "Stochastic geometry modelling and analysis for cooperative NOMA with large transmit antennas for 5G applications and beyond," *IET Commun.*, vol. 17, no. 14, pp. 1730–1740, 2023.
[32] X. Li, J. Li, Y. Liu, Z. Ding, and A. Nallanathan, "Outage performance of cooperative NOMA networks with hardware impairments," in *Proc. IEEE Glob. Commun. Conf.*, 2018, pp. 1–6.
[33] M. Can, I. Altunbas, and E. Basar, "MBM-aided uplink cooperative NOMA with hardware impairments and imperfect CSI," *IEEE Commun. Lett.*, vol. 25, no. 6, pp. 1830–1834, Jun. 2021.
[34] X. Liang, Y. Wu, D. W. K. Ng, S. Jin, Y. Yao, and T. Hong, "Outage probability of cooperative NOMA networks under imperfect CSI with user selection," *IEEE Access*, vol. 8, pp. 117921–117931, 2020.
[35] A. Amer, A.-M. Ahmad, and S. Hoteit, "Resource allocation for downlink full-duplex cooperative NOMA-based cellular system with imperfect SI cancellation and underlaying D2D communications," *Sensors*, vol. 21, no. 8, 2021, Art. no. 2768.
[36] C. Deng, M. Liu, X. Li, and Y. Liu, "Hardware impairments aware full-duplex NOMA networks over Rician fading channels," *IEEE Syst. J.*, vol. 15, no. 2, pp. 2515–2518, Jun. 2021.
[37] Z. Ding, P. Fan, and H. V. Poor, "Impact of user pairing on 5G nonorthogonal multiple-access downlink transmissions," *IEEE Trans. Veh. Technol.*, vol. 65, no. 8, pp. 6010–6023, Aug. 2016.
[38] F. Ding, H. Wang, S. Zhang, and M. Dai, "Impact of residual hardware impairments on non-orthogonal multiple access based amplify-and-forward relaying networks," *IEEE Access*, vol. 6, pp. 15117–15131, 2018.
[39] C.-B. Le, D.-T. Do, and M. Voznak, "Exploiting impact of hardware impairments in NOMA: Adaptive transmission mode in FD/HD and application in Internet-of-Things," *Sensors*, vol. 19, no. 6, 2019, Art. no. 1293.
[40] O. Alamu, T. O. Olwal, and K. Djouani, "Cooperative NOMA networks with simultaneous wireless information and power transfer: An overview and outlook," *Alexandria Eng. J.*, vol. 71, pp. 413–438, 2023.
[41] W. Han, J. Ge, and J. Men, "Performance analysis for NOMA energy harvesting relaying networks with transmit antenna selection and maximal-ratio combining over Nakagami-m fading," *IET Commun.*, vol. 10, no. 18, pp. 2687–2693, 2016.
[42] W. Zhao, R. She, and H. Bao, "Energy efficiency maximization for two-way relay assisted CR-NOMA system based on swipt," *IEEE Access*, vol. 7, pp. 72062–72071, 2019.
[43] O. Taghizadeh, A. C. Cirik, and R. Mathar, "Hardware impairments aware transceiver design for full-duplex amplify-and-forward MIMO relaying," *IEEE Trans. Wireless Commun.*, vol. 17, no. 3, pp. 1644–1659, Mar. 2018.
[44] W. M. Audu and O. O. Oyerinde, "Iteratively reweighted super-resolution channel estimation in hardware-impaired hybrid-precoded mm-Wave massive MIMO systems using dual SVD and marquardt's global search," *Digit. Signal Process.*, vol. 120, 2022, Art. no. 103308.
[45] T. A. Le and H. Y. Kong, "Effects of hardware impairment on the cooperative NOMA EH relaying network over Nakagami-m fading channels," *Wireless Pers. Commun.*, vol. 116, pp. 3577–3597, 2021.

[46] S. K. Sa and A. K. Mishra, "An uplink cooperative NOMA based on CDRT with hardware impairments and imperfect CSI," *IEEE Syst. J.*, vol. 17, no. 4, pp. 5695–5705, Dec. 2023.
[47] M. Li et al., "Effects of residual hardware impairments on secure NOMA-based cooperative systems," *IEEE Access*, vol. 8, pp. 2524–2536, 2019.
[48] O. Omarov, S. Arzykulov, G. Nauryzbayev, and T. A. Tsiftsis, "Hardware-limited cooperative swipt-enabled NOMA networks," in *Proc. IEEE 12th Int. Symp. Commun. Syst., Netw. Digit. Signal Process.*, 2020, pp. 1–6.
[49] X.-Y. Wan, R.-F. Chang, Z.-Q. Wang, and Z.-F. Fan, "Sum rate maximization for cooperative NOMA with hardware impairments," *IEICE Trans. Inf. Syst.*, vol. 104, no. 9, pp. 1399–1405, 2021.
[50] N.-L. Nguyen, S.-P. Le, A.-T. Le, N. D. Nguyen, D.-T. Do, and M. Voznak, "UAV based satellite-terrestrial systems with hardware impairment and imperfect SIC: Performance analysis of user pairs," *IEEE Access*, vol. 9, pp. 117925–117937, 2021.
[51] O. B. H. Belkacem, M. L. Ammari, and R. Dinis, "Performance analysis of NOMA in 5G systems with HPA nonlinearities," *IEEE Access*, vol. 8, pp. 158327–158334, 2020.
[52] X. Li, M. Liu, D. Deng, J. Li, C. Deng, and Q. Yu, "Power beacon assisted wireless power cooperative relaying using NOMA with hardware impairments and imperfect CSI," *AEU- Int. J. Electron. Commun.*, vol. 108, pp. 275–286, 2019.
[53] M. H. N. Shaikh, V. A. Bohara, A. Srivastava, and G. Ghatak, "A downlink RIS-aided NOMA system with hardware impairments: Performance characterization and analysis," *IEEE Open J. Signal Process.*, vol. 3, pp. 288–305, 2022.
[54] D.-T. Do and A.-T. Le, "NOMA based cognitive relaying: Transceiver hardware impairments, relay selection policies and outage performance comparison," *Comput. Commun.*, vol. 146, pp. 144–154, 2019.
[55] D.-T. Do and T.-T. T. Nguyen, "Impacts of imperfect SIC and imperfect hardware in performance analysis on AF non-orthogonal multiple access network," *Telecommun. Syst.*, vol. 72, no. 4, pp. 579–593, 2019.
[56] D. Dinh-Thuan and T. N. Tu-Trinh, "Exploiting system performance in AF non-orthogonal multiple access network under impacts of imperfect sic and imperfect hardware," *Phys. Commun.*, vol. 38, 2020, Art. no. 100912.
[57] M. Ahmed et al., "Cooperative backscatter NOMA with imperfect SIC: Towards energy efficient sum rate maximization in sustainable 6G networks," *J. King Saud Univ.- Comput. Inf. Sci.*, vol. 34, no. 10, pp. 7940–7947, 2022.
[58] G. Li and D. Mishra, "Cooperative NOMA networks: User cooperation or relay cooperation?," in *Proc. IEEE Int. Conf. Commun.*, 2020, pp. 1–6.
[59] D. Zhang, Y. Liu, Z. Ding, Z. Zhou, A. Nallanathan, and T. Sato, "Performance analysis of non-regenerative massive-MIMO-NOMA relay systems for 5G," *IEEE Trans. Commun.*, vol. 65, no. 11, pp. 4777–4790, Nov. 2017.
[60] W. Xie, X. Xia, Y. Xu, K. Xu, and Y. Wang, "Massive MIMO full-duplex relaying with hardware impairments," *J. Commun. Netw.*, vol. 19, no. 4, pp. 351–362, 2017.
[61] F. Kara and H. Kaya, "Improved user fairness in decode-forward relaying non-orthogonal multiple access schemes with imperfect SIC and CSI," *IEEE Access*, vol. 8, pp. 97540–97556, 2020.
[62] L. May Taniguchi and T. Abrao, "Stochastic channel models for massive and extreme large multiple-input multiple-output systems," *Trans. Emerg. Telecommun. Technol.*, vol. 31, no. 9, 2020, Art. no. e4099.
[63] K. Zheng, S. Ou, and X. Yin, "Massive MIMO channel models: A survey," *Int. J. Antennas Propag.*, vol. 2014, no. 1, 2014, Art. no. 848071.
[64] C. Liao et al., "Geometry-based stochastic model and statistical characteristic analysis of cell-free massive MIMO channels," *Secur. Commun. Netw.*, vol. 2022, no. 1, 2022, Art. no. 4730044.
[65] Y. Xie, B. Li, X. Zuo, M. Yang, and Z. Yan, "A 3D geometry-based stochastic model for 5G massive MIMO channels," in *Proc. IEEE 11th Int. Conf. Heterogeneous Netw. Qual., Rel., Secur. Robustness*, 2015, pp. 216–222.
[66] Á. O. Martínez, P. Eggers, and E. De Carvalho, "Geometry-based stochastic channel models for 5G: Extending key features for massive MIMO," in *Proc. IEEE 27th Annu. Int. Symp. Pers., Indoor, Mobile Radio Commun.*, 2016, pp. 1–6.
[67] S. Tweneboah-Koduah, E. A. Affum, K. Agyemang-Prempeh Agyekum, S. A. Ajagbe, and M. O. Adigun, "Performance of cooperative relay NOMA with large antenna transmitters," *Electronics*, vol. 11, no. 21, 2022, Art. no. 3482.
[68] S. Tweneboah-Koduah, E. A. Affum, K. S. O. Kwakye, and O. A. Antwi, "Decode and forward coding scheme for cooperative relay NOMA system with cylindrical array transmitter," *Int. J. Adv. Comput. Sci. Appl.*, vol. 13, no. 10, 2022, Art. no. 0131090.
[69] Y. Liu, X. Li, F.-K. Gong, and Y. Lin, "TDD reciprocity compensation for massive MIMO system with iterative calibration," in *Proc. IEEE 8th Int. Conf. Wireless Commun. Signal Process.*, 2016, pp. 1–4.
[70] B. Li, L.-L. Yang, R. G. Maunder, S. Sun, and P. Xiao, "Multicarrier-division duplex for solving the channel aging problem in massive MIMO systems," *IEEE Trans. Veh. Technol.*, vol. 72, no. 2, pp. 1940–1954, Feb. 2023.
[71] C.-F. Liu, M. Maso, S. Lakshminarayana, C.-H. Lee, and T. Q. Quek, "Simultaneous wireless information and power transfer under different CSI acquisition schemes," *IEEE Trans. Wireless Commun.*, vol. 14, no. 4, pp. 1911–1926, Apr. 2014.
[72] J. Meredith, "Study on channel model for frequency spectrum above 6 GHz," 3GPP, Tech. Rep. TR 38.900, Jun. 2016.
[73] J. Salo et al., "Universal mobile telecommunications system (UMTS); spatial channel model for multiple input multiple output (MIMO) simulations," Eur. Telecommun. Standards Inst., Nice, French, Tech. Rep. GT, 25, 16.0.0, 2020.
[74] E. Assiimwe and Y. W. Marye, "A stochastic confocal elliptic-cylinder channel model for 3D MIMO in millimeter-wave high-speed train communication system," *Electronics*, vol. 11, no. 13, 2022, Art. no. 1948.
[75] K. Guan et al., "Channel characterization and capacity analysis for THz communication enabled smart rail mobility," *IEEE Trans. Veh. Technol.*, vol. 70, no. 5, pp. 4065–4080, May 2021.
[76] K. Guan et al., "Channel sounding and ray tracing for THz channel characterization," in *Proc. IEEE 13th U.K.-Europe-China Workshop Millimetre-Waves Terahertz Technol.*, 2020, pp. 1–3.
[77] Q.-U.-A. Nadeem, A. Kammoun, M. Debbah, and M.-S. Alouini, "3D massive MIMO systems: Modeling and performance analysis," *IEEE Trans. Wireless Commun.*, vol. 14, no. 12, pp. 6926–6939, Dec. 2015.
[78] A. E. Ampoma, G. Wen, Y. Huang, K. O. Gyasi, P. I. Tebe, and K. Ntiamoah-Sarpong, "Spatial correlation models of large-scale antenna topologies using maximum power of offset distribution and its application," *IEEE Access*, vol. 6, pp. 36295–36304, 2018.
[79] Q.-U.-A. Nadeem, A. Kammoun, M. Debbah, and M.-S. Alouini, "Spatial correlation characterization of a uniform circular array in 3D MIMO systems," in *Proc. IEEE 17th Int. Workshop Signal Process. Adv. Wireless Commun.*, 2016, pp. 1–6.
[80] C. T. Neil, M. Shafi, P. J. Smith, and P. A. Dmochowski, "On the impact of antenna topologies for massive MIMO systems," in *Proc. IEEE Int. Conf. Commun.*, 2015, pp. 2030–2035.
[81] Y. Cheng, K. H. Li, Y. Liu, K. C. Teh, and H. Vincent Poor, "Downlink and uplink intelligent reflecting surface aided networks: NOMA and OMA," *IEEE Trans. Wireless Commun.*, vol. 20, no. 6, pp. 3988–4000, Jun. 2021.
[82] E. Bjornson, M. Matthaiou, and M. Debbah, "A new look at dual-hop relaying: Performance limits with hardware impairments," *IEEE Trans. Commun.*, vol. 61, no. 11, pp. 4512–4525, Nov. 2013.
[83] Z. Wang, Z. Peng, Y. Pei, and H. Wang, "Performance analysis of cooperative NOMA systems with incremental relaying," *Wireless Commun. Mobile Comput.*, vol. 2020, no. 1, 2020, Art. no. 4915638.
[84] F. Kara and H. Kaya, "BER performances of downlink and uplink NOMA in the presence of SIC errors over fading channels," *IET Commun.*, vol. 12, no. 15, pp. 1834–1844, 2018.
[85] M. Shen, Z. Huang, X. Lei, and L. Fan, "BER analysis of NOMA with max-min relay selection," *China Commun.*, vol. 18, no. 7, pp. 172–182, Jul. 2021.

EMMANUEL AMPOMA AFFUM received the B.S. degree in electronics and communication engineering from the Kwame Nkrumah University of Science and Technology, Kumasi, Ghana, in 2007, the M.Tech. degree in communication systems from SRM University Chennai, Chennai, India, in 2009, and the Ph.D. degree in information and communication engineering from the Center for RFIC and System Technology, School of Communication and Information Engineering, University of Electronic Science and Technology of China, Chengdu, China, in 2018. He is currently with the Faculty of Electrical and Electronic Engineering, Kwame Nkrumah University of Science and Technology, Kumasi, Ghana. He has authored or coauthored several journal papers and conference papers. His research interests include the field of wireless communication and signal processing with a particular focus on array processing, channel modeling, and performance analysis of wireless communication systems. Since 2023, The World Academy of Sciences for the Advancement of Science in Developing Countries has awarded him the TWAS-UNESCO Associateships Scholarship at Centers of Excellence in the South. He was the recipient of the Chinese Outstanding International Student Scholarship in 2017.

SAMUEL TWENEBOAH-KODUAH received the Bachelor of Science degree in telecommunication engineering from the Kwame Nkrumah University of Science and Technology, Kumasi, Ghana, in 2010, the Master of Engineering (M.Eng.) degree in information and communication engineering from Hanbat National University, Daejeon, South Korea, in 2013. He is currently working toward the Ph.D. degree with the Kwame Nkrumah University of Science and Technology. He is also a Lecturer with the Department of Computer and Electrical Engineering, University of Energy and Natural Resources, Sunyani, Ghana. He has authored or coauthored several journal articles and conference papers, providing substantial contributions to his area of specialization. His research interests include wireless channel modelling, signal processing, 5G and wireless communication systems, machine learning, and IoT.

OWUSU AGYEMAN ANTWI received the bachelor's degree from Ghana Communication Technology University, Accra, Ghana, in 2014, and the master's degree from Ghana Communication Technology University and Kwame Nkrumah University of Science and Technology, Kumasi, Ghana, in 2018. He is currently a Lecturer with Ghana Communication Technology University and final-year Ph.D. candidate with Kwame Nkrumah University of Science and Technology. Throughout his academic career, he has authored or coauthored few journal articles and conference papers, contributing valuable insights to his field of expertise. His research interests are not just focused on cutting-edge communication technologies, but also on their potential to revolutionize wireless communication networks. His areas of expertise include reconfigurable intelligent surfaces, hybrid radio frequency-visible light communication systems, and integration of communication and sensing systems.

BENJAMIN ASUBAM WEYORI (Member, IEEE) received the B.Sc. degree in computer science, the M.Phil. degree in computer engineering, and the Ph.D. degree in computer engineering. He is currently an Associate Professor and Head of the Department of Computer and Electrical Engineering, University of Energy and Natural Resources, Sunyani, Ghana. He has authored many research articles and books on computer vision, machine learning, quantum computing, Internet of Things (IoTs), block chain technology, high-speed optical communication systems and devices, and wireless communication systems. His research interests include computer vision, machine learning, quantum computing, Internet of Things (IoT), block chain technology, high-speed optical communication systems and devices, and wireless communication systems. He is an editorial member and reviewer of several internationally reputed journals. He is a Member of many international affiliations, including the Ghana Institution of Engineering (GhIE) and International Association of Engineers (IAENG).

WILLIE OFOSU (Life Member, IEEE) is currently a Professor of engineering with University College, Pennsylvania State University, University Park, PA, USA. His research interest in globalization and technology transfer has led to supporting the development of a Bachelor of Science Program in Telecommunications Engineering at Kwame Nkrumah University of Science and Technology (KNUST), Kumasi, Ghana. He has also assisted the Master of Technology Program at the University of Education-Kumasi Campus, Ghana.